International Journal of Nanomedicine

Dovepress
open access to scientific and medical research

Open Access Full Text Article

ORIGINAL RESEARCH

A Biomimetic Smart Nanoplatform as "Inflammation Scavenger" for Regenerative Therapy of Periodontal Tissue

Poyu Chen[1–3,*], Chuangwei Zhang[1–3,*], Ping He[4], Shengyuan Pan[1–3], Wenjie Zhong[1–3], Yue Wang[1–3], Qingyue Xiao[1–3], Xinyan Wang[1–3], Wenliang Yu[1–3], Zhangmin He[1–3], Xiang Gao[1–3], Jinlin Song[1–3]

[1]College of Stomatology, Chongqing Medical University, Chongqing, 401147, People's Republic of China; [2]Chongqing Key Laboratory of Oral Diseases and Biomedical Sciences, Chongqing, 401147, People's Republic of China; [3]Chongqing Municipal Key Laboratory of Oral Biomedical Engineering of Higher Education, Chongqing, 401147, People's Republic of China; [4]Department of Stomatology, Dazhou Central Hospital, Dazhou, SiChuan, 635000, People's Republic of China

*These authors contributed equally to this work

Correspondence: Xiang Gao; Jinlin Song, Chongqing Key Laboratory for Oral Diseases and Biomedical Sciences, Chongqing, 401147, People's Republic of China, Tel/Fax +86 23 88860105; Tel/Fax +86 23 88860026, Email xiangg@hospital.cqmu.edu.cn; songjinlin@hospital.cqmu.edu.cn

Introduction: The functional reconstruction of periodontal tissue defects remains a clinical challenge due to excessive and prolonged host response to various endogenous and exogenous pro-inflammatory stimuli. Thus, a biomimetic nanoplatform with the capability of modulating inflammatory response in a microenvironment-responsive manner is attractive for regenerative therapy of periodontal tissue.

Methods: Herein, a facile and green design of engineered bone graft materials was developed by integrating a biomimetic apatite nanocomposite with a smart-release coating, which could realize inflammatory modulation by "on-demand" delivery of the anti-inflammatory agent through a pH-sensing mechanism.

Results: In vitro and in vivo experiments demonstrated that this biocompatible nanoplatform could facilitate the clearance of reactive oxygen species in human periodontal ligament stem cells under inflammatory conditions via inhibiting the production of endogenous proinflammatory mediators, in turn contributing to the enhanced healing efficacy of periodontal tissue. Moreover, this system exhibited effective antimicrobial activity against common pathogenic bacteria in the oral cavity, which is beneficial for the elimination of exogenous pro-inflammatory factors from bacterial infection during healing of periodontal tissue.

Conclusion: The proposed strategy provides a versatile apatite nanocomposite as a promising "inflammation scavenger" and propels the development of intelligent bone graft materials for periodontal and orthopedic applications.

Keywords: periodontal bone regeneration, pH-responsive, inflammatory modulation, antibacterial activity, biomimetic nanoplatform

Introduction

With the growing aging population, periodontal disease is becoming a global public health concern and financial burden, which affects around 538 million people worldwide.[1,2] Due to the destruction of periodontal tissue, individuals suffering from severe periodontal disease are at risk of tooth loss and masticatory dysfunction, which have a serious impact on quality of life.[3] For tooth retention, regenerative therapy such as guided bone regeneration (GBR) is widely applied in clinics to restore the destroyed alveolar bone tissue in periodontal disease.[4] Nevertheless, the efficacy of such treatment is often challenged by host responses to various exogenous and endogenous pro-inflammatory stimuli, including bacterial infection,[5] surgical trauma,[6] excessive occlusal stress,[7] and artificial graft materials.[8] Mounting evidence indicates that inflammation serves as a bidirectional signal during the healing process of damaged periodontal tissue. An appropriate host inflammatory response is essential for unimpeded tissue repair, whereas excessive and

Received: 6 August 2022
Accepted: 25 October 2022
Published: 4 November 2022

Graphical Abstract

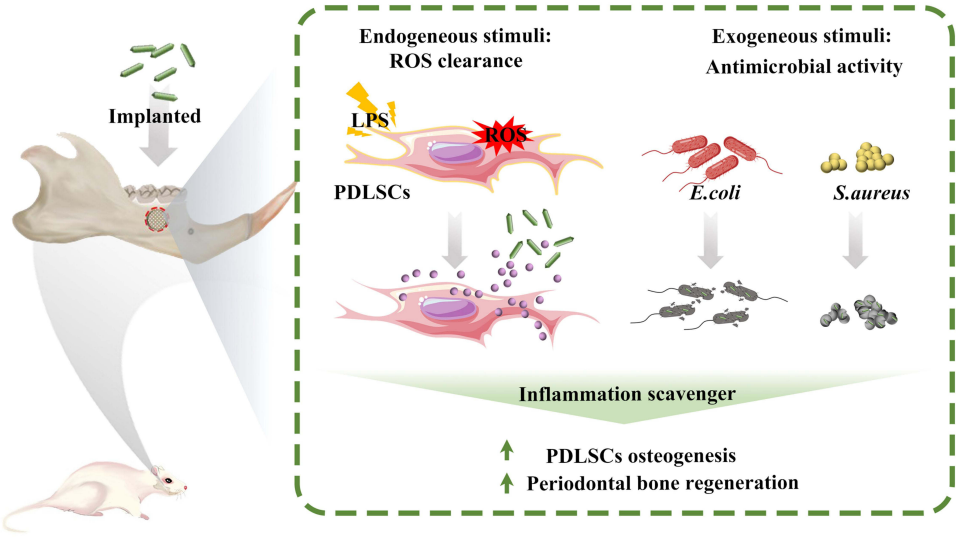

prolonged inflammation could lead to incomplete or failed tissue healing.[9,10] Therefore, to achieve a favorable outcome in periodontal regenerative treatment, the self-tuning regulation of the host response to various proinflammatory stimuli during the healing stage is in great demand; however, this remains a challenge in the field of periodontal medicine.[11]

Reconstruction of periodontal tissue after regenerative therapy is a complex biological process that involves three partially overlapping phases: the inflammatory phase, the repair phase, and the remodeling phase.[12,13] During the initial inflammation phase, a variety of pro-inflammatory mediators such as *TNF-α, INF-γ*, and *IL-1β* are largely released by tissue-resident cells such as immune cells, endothelial cells, fibroblasts, and stem cells in response to pathogen-associated molecular patterns (eg, bacterial endotoxin, and lipopolysaccharide) and damage-associated molecular patterns (eg, tissue injury byproducts), which could contribute to the elimination of invading pathogens, necrotic tissue, and the provisional fibrin matrix via the immune system.[14–16] With the clearance of pro-inflammatory stimuli, the resolution of inflammation, which is characterized by the downregulation of pro-inflammatory cytokines and the upregulation of anti-inflammatory mediators (eg, *IL-4, IL-10* and *CCL2*), will be activated for further advancement of the healing process.[17–19] During this transition, any cues that cause persistence of stimuli or incomplete resolution of inflammation could result in the accumulation of pro-inflammatory cytokines at local wound sites, eventually hampering the regeneration and reconstruction of damaged tissue. Additionally, the accumulation of pro-inflammatory cytokines is also known to be a potent inducer of oxidative stress damage in periodontal tissue.[20] Therefore, ensuring a timely switch of host response from a pro-inflammatory to an anti-inflammatory phenotype at local wound sites is pivotal for creating a pro-regenerative tissue environment. To this end, tissue engineering strategies for the local delivery of anti-inflammatory cytokines and drugs in a "smart" inflammatory stimuli-responsive manner have been increasingly pursued in recent years, which are believed to be an effective solution to enhance the success rate of regenerative therapy.[21,22]

Among various scaffold materials, apatite-based nanomaterials are considered an ideal drug delivery system for the regenerative therapy of periodontal tissue due to their chemical and biomechanical similarity to the mineral phase of natural bone tissue.[23–26] However, traditional drug-loading approaches such as physical adsorption and chemical bonding cannot endow apatite nanomaterials with the capacity to release therapeutic cargo in response to external stimuli.[27] Moreover, synthetic apatite nanocrystals with irregular size, morphology, and crystallinity are susceptible to induce a foreign body reaction characterized by local chronic inflammation, imposing a negative impact on tissue repair.[28,29] To

address these issues, recent efforts have been focused on developing a biomimetic smart apatite-based nanoplatform with the capability of modulating inflammatory response in an external stimuli-responsive manner for enhanced regeneration of periodontal tissue after implantation.

Taking the above discussion into consideration, herein, we developed an integrated set of strategies that combine biomimetic apatite nanocomposites with post-fabrication functionalization. Research works included (1) synthesizing a kind of apatite nanocomposite using polydopamine as a template, which shows physicochemical properties similar to inorganic components in bone tissue, and (2) constructing a smart-release coating on the surface of biomimetic apatite nanocrystals for local delivery of aspirin (a widely used anti-inflammatory agent) through a pH-sensing mechanism. To our knowledge, this is the first report on the design of a biomimetic smart apatite-based nanoplatform that could intelligently regulate the host inflammatory response by "on-demand" delivery of the anti-inflammatory agent. For application in periodontal tissue engineering, the bioactivity of this engineered apatite-based nanoplatform in terms of antibacterial effect, anti-inflammatory effect, and osteo-promoting effect was comprehensively assessed in vitro and in vivo. It is believed that our study sheds new light on the design of biomimetic nanoplatforms with "smart" surface behavior for the regulation of host inflammatory response, which shows a promising potential in the field of periodontal and orthopedic regenerative medicine.

Materials and Methods

Construction and Characterization of Biomimetic Smart Nanoplatform

Firstly, biomimetic apatite nanocomposites (tHA) were synthesized using polydopamine as a template based on a previously reported method.[30] Briefly, dopamine hydrochloride (Sigma, USA) was added to a $CaCl_2$ (Aladdin, China) solution at a concentration of 2 mg/mL. Then, Na_2HPO_4 (Aladdin, China) solution was added to the $CaCl_2$-dopamine mixture drop by drop with continuous stirring until a Ca/P ratio of 1.67 was achieved. The reaction was processed under pH 8.5 for 12 h at 60°C. After aging for 1 d at 37°C, the precipitate was harvested by centrifugation and dried at 60°C for further application. To prepare ASA@tHALLG nanocomposites, 100 mg of tHA powder was added to 10 mL of poly(L-lysine) (PLL, 1%, Aladdin, China) solution. The mixture was stirred overnight at room temperature (RT). Then, the collected PLL-modified tHA was alternatively reacted with negatively charged carboxymethyl chitosan (CMC, 1%, Aladdin, China) solution and positively charged PLL (1%) solution for 5 min at RT followed by a washing procedure. Aspirin was loaded into the coatings during the assembly process. After a 10-cycle deposition, the ASA-laden CMC/PLL assembly was crosslinked with 1% genipin solution for 8 h at RT. The obtained product, denoted as ASA@tHALLG, was freeze-dried in a lyophilizer (FD-D12N-80, KuanSons, China) for 24–32 h, and then kept at −20°C for further study. The apatite nanocomposites without ASA loading and genipin crosslinking were denoted as tHALLG and ASA@tHALL, respectively.

The morphology and size of the prepared apatite nanocomposites were examined by transmission electron microscopy (TEM, 7500, Hitachi, Japan) at 100 kV. An X-ray photoelectron spectrometer microprobe (Thermo Fisher, USA) was used to analyze chemical and elemental composition. A spectra analysis was conducted using CasaXPS software. Fourier transform infrared (FTIR) spectroscopy was performed using a Thermo Scientific Nicolet 6700 spectrometer (Thermo Scientific Inc., USA) to identify the chemical groups present in the nanocomposites. The release kinetics of ASA from ASA@tHALLG was studied as in previous publications.[31] Briefly, the prepared apatite nanocomposites were placed in a dialysis bag containing 1 mL of buffer solutions (either pH 5.5 or 7.4) and further immersed in a beaker filled with the same buffer solutions for 18 days at 37°C. At each preset time point, 1 mL of release medium was removed from the beaker and subsequently replaced with 1 mL of the same fresh buffer. The collected release medium was assayed at 267 nm using a SpectraMax iD5 Multi-mode microplate reader (Molecular Devices, USA). The released amount of ASA at each time point was calculated from the standard curve established before.

Cell Co-Culture

hPDLSCs were kindly provided by the Oral Stem Cell Bank (Beijing, China) and maintained in α-MEM media (Gibco, USA) containing 1% penicillin/streptomycin (Gibco, USA) and 10% fetal bovine serum (Gibco, USA) under standard

culture conditions (37°C, 5% CO_2, and 95% humidity). To induce osteogenic differentiation of the stem cells, the growth media was changed to osteoinductive media, which was prepared by the addition of 50 μg/mL ascorbic acid, 10 mM β-glycerophosphate, and 100 nM dexamethasone into growth media. Culture media containing lipopolysaccharide (LPS, 10 μg/mL, Sigma, USA) was used to induce cellular inflammatory response. The culture media was changed every 2–3 days.

Cell Adhesion Evaluation

The early adhesion of hPDLSCs subjected to the apatite nanocomposites was evaluated by fluorescein diacetate (FDA) staining (Sigma, USA). After seeding for 3 h, cells were incubated in α-MEM media containing 5 mg/mL FDA for 5 min at RT. Then, the stained cells were washed with fresh α-MEM media and immediately observed under a fluorescence microscope.

The morphology of the hPDLSCs exposed to apatite nanocomposites was examined by field emission scanning electron microscopy (SEM, SU8010, Hitachi, Japan). At 24 h after coculture, the cells were fixed with 2.5% glutaraldehyde at 4°C for 2 h and dehydrated in gradient ethanol. Next, the cells were dried at the critical point and gold-sputtered for SEM observation. For cytoskeleton staining, the cells were fixed with 4% paraformaldehyde (PFA) for 10 min, permeabilized with 0.1% Triton X-100 for 5 min, and stained with 1 μg/mL FITC-phalloidin (Sigma, USA) for 30 min at RT. After that, the stained cells were mounted with DAPI and observed under a fluorescence microscope.

Cell Proliferation Evaluation

Cell Counting Kit-8 (CCK-8, Beyotime, China) was used to assess cell proliferation when hPDLSCs were cocultured with apatite nanocomposites following the manufacturer's protocol. Briefly, at 1, 3, and 5 days after cell seeding, the culture media was changed with CCK-8 working solution and incubated for 2 h at 37°C. Then, the absorbance of the supernatant (100 μL) from each well was recorded at 450 nm using a microplate reader (EnSpire, PerkinElmer, USA).

Lactate Dehydrogenase Assay

The cytotoxicity of the nanomaterials was assessed using a lactate dehydrogenase (LDH) assay kit (Beyotime, China). At 24 h after cell seeding, the supernatant from each group was tested following the manufacturer's protocol.

Reactive Oxygen Species Assay

A dichlorofluorescein diacetate staining kit (Beyotime, China) was used to assess intracellular ROS. At 24 h after cell seeding, cells in each group were stained according to the manufacturer's protocol and further investigated by fluorescence microscopy.

Alkaline Phosphatase Activity Evaluation

The alkaline phosphatase (ALP) activity of cells was evaluated using an ALP assay kit (Nanjing Jiancheng, China). Briefly, after osteogenic induction for 7 days, the cells in each group were treated with 1% Triton X-100. Afterwards, the cell lysates (30 μL) were collected and measured for ALP activity following the manufacturer's protocol. To visualize ALP expression, the cells were fixed with 4% PFA for 10 min at RT and stained using a BCIP/NBT ALP color development Kit (Beyotime, China).

Alizarin Red S Staining

After osteogenic induction for 21 days, samples were fixed with 60% isopropyl alcohol for 1 min at RT. Then, the fixed samples were washed with ddH_2O and stained with 2% alizarin red S (ARS) (Sigma, USA) for 10 min to evaluate calcium deposition. After that, the stained calcium nodules were eluted with cetylpyridinium chloride solution (10%) for 1 h at RT. The absorbance of the eluant from each group was recorded at 550 nm using a microplate reader.

Immunofluorescent Staining

After osteogenic induction for 14 days, cells cocultured with the prepared materials were fixed with 4% PFA. Then, the cells were treated with 0.1% Triton X-100 and blocked with 5% BSA. Afterward, the cells were treated with antibodies OPN (1:500, anti-mouse, Santa Cruz, USA) and RUNX2 (1:500, anti-rabbit, CST, USA) separately overnight at 4°C. After thoroughly washing with PBS, the cells were stained with goat anti-mouse IgG (H+L) cross-adsorbed secondary antibody (1:2000, Invitrogen, USA) and goat anti-rabbit IgG (H+L) cross-adsorbed secondary antibody (1:500, Invitrogen, USA) for 1 h. Finally, the cells were placed in a fluorescent mounting medium with DAPI for further observation under the fluorescence microscope.

Quantitative Real-Time Polymerase Chain Reaction

Total RNA was extracted using the RNAiso Plus Kit (Takara, Japan) and reverse-transcribed into cDNA using the PrimeScript RT reagent kit (Takara, Japan) according to the manufacturer's instructions. Quantitative real-time polymerase chain reaction (RT-qPCR) was conducted using SYBR Premix Ex Taq II (Takara, Japan) on the CFX96 Touch Real-Time PCR detection system (Bio-Rad, USA). The relative expression of the target genes was determined using the ΔΔCt method. The primers used in this study are listed in Table S1.

In vivo Experiment

Animal experiments were approved by the Animal Ethics Committee of Chongqing Medical University (CQHS-REC -2021 (LSNo.47)) and performed according to the National Institutes of Health (NIH) guidelines for the Care and Use of Laboratory Animals. In this study, 12 male Sprague-Dawley rats weighing 200–250 g were used to establish the root fenestration model.[32] As previously described, rats were anesthetized with 10% chloral hydrate solution (30 mg/100 g) via intraperitoneal injection after adaptive feeding for 1 week.[33] Then, the hair around the mandibular angle regions was shaved, and the skin was disinfected for further exposure of the mandible according to the standard.[32] On the exposed buccal plates covering the periapical area of the first and second molars, bone defects with a diameter of 3 mm and a depth of 1 mm were created using a dental trephine and implanted with the prepared materials. The masseter muscle was repositioned to keep the material at the defect area. After that, the overlying soft tissues were closed and treated with antibiotic ointment. To determine the growth rate of the new bone tissues, calcein (20 mg/kg, Sigma, USA) was injected subcutaneously at 14 days and 4 days before sacrifice. At four weeks after surgery, all animals were sacrificed. The mandible specimens were harvested and fixed in 4% PFA for further evaluation. To assess the 3D micro-architecture of newly formed bone tissues, high-resolution images of the fixed specimens were obtained and analyzed using a μCT scanner (VivaCT 40, Scanco Medical, Switzerland). After the μCT analysis, both decalcified and undecalcified specimens were prepared for histological evaluation. Undecalcified specimens were sequentially dehydrated in a graded ethanol series and then embedded in plastic resin for sectioning to detect fluorochrome labels. The paraffin-embedded decalcified specimens were sectioned for further histological analyses, including H&E staining, Masson-trichrome staining, and immunohistochemical staining of osteogenic and inflammatory markers.

Antibacterial Assay

To assess the broad-spectrum antibacterial activity of engineered apatite nanocomposite, Gram-negative *Escherichia coli* (*E. coli*) and Gram-positive *Staphylococcus aureus* (*S. aureus*), the two common bacteria in oral cavity responsible for post-surgical infection, were used to investigate the antibacterial activity of the prepared materials. Briefly, the bacterial strains cocultured with materials were grown in a nutrient broth medium under standard anaerobic conditions (5%, CO_2, 37°C). At scheduled time points, the culture media was removed, and bacterial adhesion was assessed using Microbial Viability Assay Kit-WST (Dojindo, Japan) and a LIVE/DEAD BacLight bacterial viability kit (Invitrogen, USA), according to the manufacturers' protocols. Afterwards, the bacteria in each group were fixed for further observation under SEM.

In vivo antibacterial experiments were carried out as previously described.[34] After adaptive feeding for one week, eight male C57BL/6 mice (6–8 weeks) were anesthetized with 4% chloral hydrate (i.p.) for subcutaneous injection of

100 μL bacteria solution (*S. aureus*, 1 × 10^7 CFU/mL) with or without ASA@tHALLG nanocomposites (final concentration was 3 μg/μL). Twenty-four hours later, the mice were euthanized, and the subcutaneous tissue fluids were diluted and spread onto agar plates. The surrounding tissue was harvested and fixed in 4% PFA for histological investigation.

Statistical Analysis

All the data are expressed as mean ± SD. Significant differences among groups are determined using a one-way analysis of variance (ANOVA), followed by Tukey's post-hoc test for multiple comparisons. A p value <0.05 was considered to indicate statistical significance.

Results and Discussion

Construction and Characterization of Biomimetic Smart Nanoplatform

Figure 1 shows the preparation of ASA@tHALLG nanocomposite with anti-inflammatory and anti-bacterial properties for regenerative therapy of periodontal bone tissue. In this study, polydopamine (pDA) was employed as a template to synthesize biomimetic apatite composite (denoted as tHA). Then, a genipin crosslinked CMC/PLL (GCP) assembly loaded with aspirin was constructed onto the surface of tHA via the covalent linkage between catechol moieties in pDA and the amine groups of PLL.[35–37] After that, many kinds of techniques were utilized to characterize the changes during the synthesis of the ASA@tHALLG nanocomposite. The morphology of the prepared apatite nanocomposite post-fabrication was observed via TEM, as shown in Figure 2A. It was obvious that the agglomerated nano-sized apatite crystals were in the form of a plate-like structure, which was similar to the natural apatite crystal in bone tissue.[38] It is

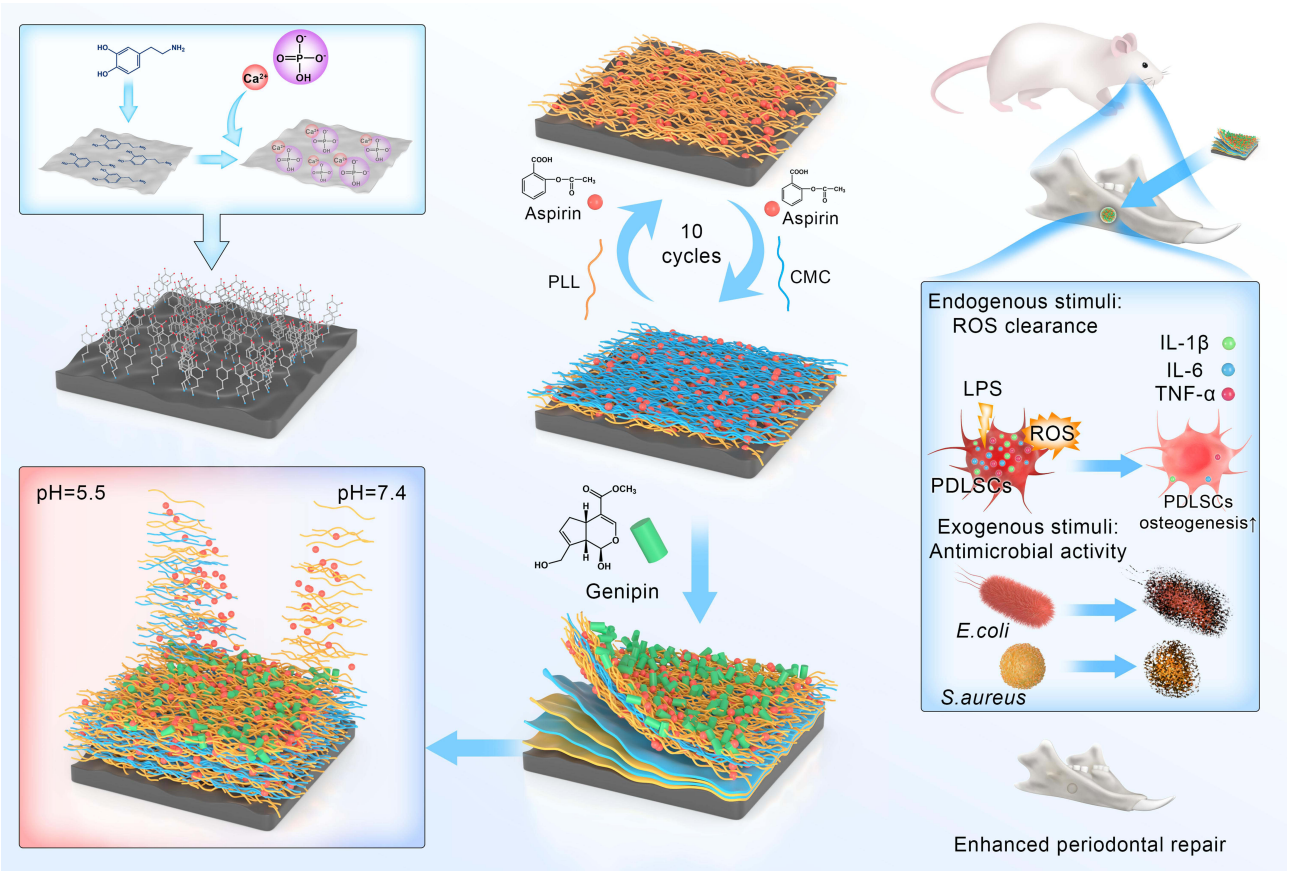

Figure 1 Schematic illustration of synthesis of biomimetic smart nanoplatform with pH-responsive anti-inflammatory effect as graft materials. Due to the enhanced bioactivity in regulation of local host inflammatory response and prevention of microbial infection, the engineered apatite nanocomposite shows a promising potential for regenerative therapy of periodontal tissue.

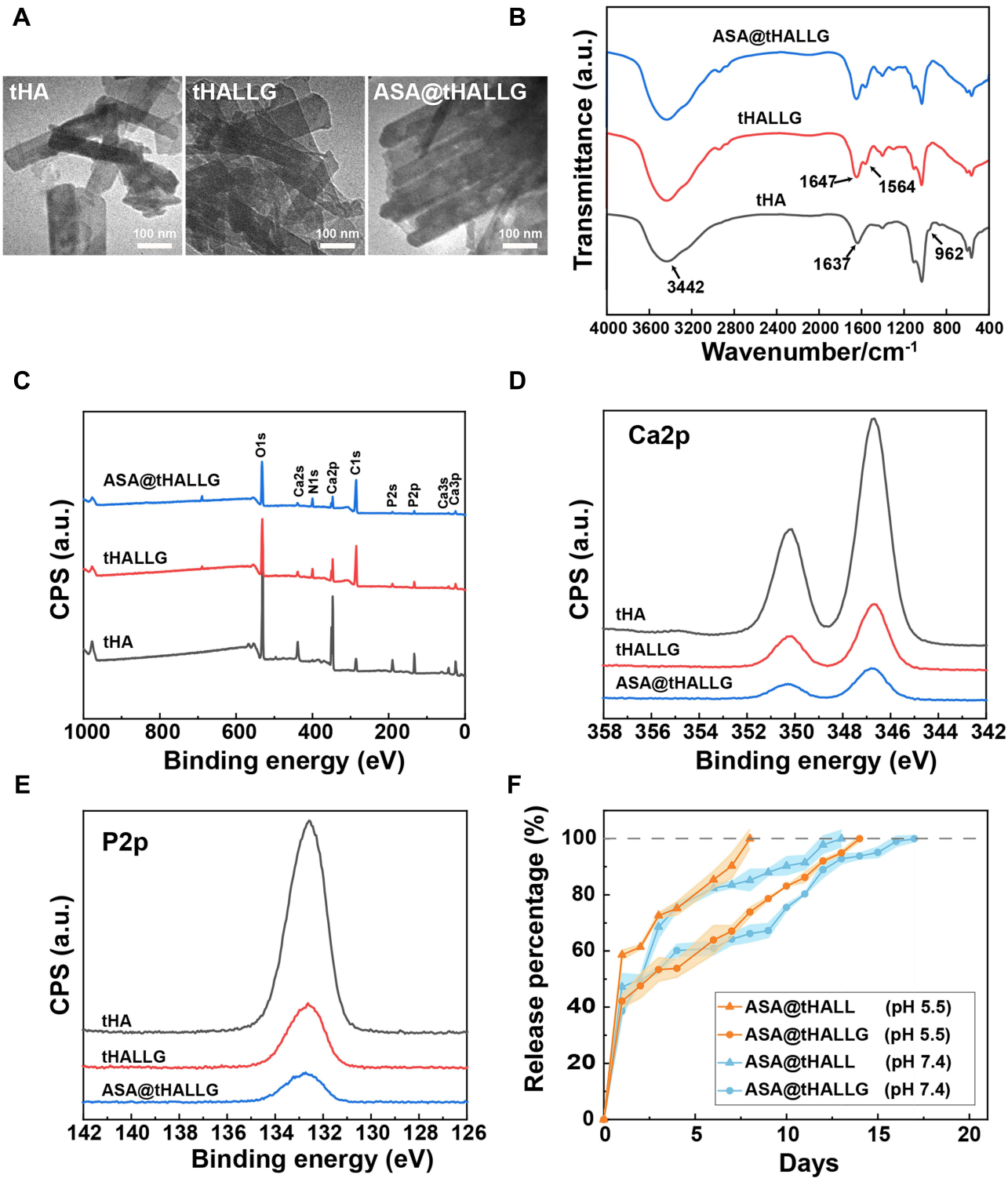

Figure 2 Characterization of synthesized biomimetic smart nanoplatform. (**A**) TEM observation of tHA, tHALLG and ASA@tHALLG nanocomposites. Scale bars = 100 nm. (**B**) FTIR spectra, (**C**) XPS wide spectra, (**D**) typical Ca 2p and (**E**) P 2p spectra for tHA, tHALLG and ASA@tHALLG nanocomposites. (**F**) In vitro release of aspirin from ASA@tHALL and ASA@tHALLG in different buffers.

noteworthy that a translucent coating (light gray outer layer) was detected on the surface of tHALLG and ASA@tHALLG in comparison with tHA, providing direct evidence for the presence of the GCP assembly on the apatite crystals.

To further prove the successful synthesis of ASA@tHALLG, the chemical constituents and states of the engineered nanocomposites were characterized by FTIR and XPS. As shown in Figure 2B, the characteristic peak for the apatite crystals was recorded at 962 cm^{-1}, which belongs to the nondegenerate symmetric stretching mode of PO_4^{3-}.[39] Also, broad bands around 3442 cm^{-1} and 1637 cm^{-1} were observed due to the absorbed H_2O in tHA.[40] After constructing the GCP assembly on the surface of tHA, a new peak at 1564 cm^{-1} appeared, which was ascribed to amide II (mainly from in-plane N-H bending).[41] Moreover, the peak at 1647 cm^{-1} was intensified, which may be due to the superimposed vibration of H_2O and an amide I band that is mainly associated with the C=O stretching vibration.[42,43] Although the spectra of ASA@tHALLG showed no obvious difference from that of tHALLG, these results suggested that the GCP assembly was successfully covalently bonded on the surface of tHA, which was further confirmed by XPS investigation. As shown in Figure 2C, apart from major atomic elements carbon, oxygen, calcium, and phosphorus, a weak nitrogen peak at 399 eV was recorded in the tHA nanocomposite, suggesting the presence of pDA. After coating the GCP assembly on the surface of tHA, the nitrogen signal was enhanced due to the contribution of the abundant amide groups in the assembly; this was accompanied by decreased signals for Ca 2p and P 2p, which was also found in corresponding high-resolution spectra (Figures S1, 2D and E). Compared to tHALLG, the signals for Ca 2p and P 2p were further decreased in ASA@tHALLG (Figure 2D and E). Additionally, according to the elementary composition analysis, the content of Ca 2p and P 2p decreased from 4.69% to 2.98% and from 3.93% to 2.3%, respectively, indicating the successful loading of aspirin into the GCP assembly. It is noteworthy that compared to the stoichiometric ratio (1.67) in apatite,[44] a lower Ca/P ratio (1.30) was detected in the tHA nanocomposites, implying a calcium-deficient state in the tHA nanocrystals. Previous studies reported that the Ca/P atomic ratio of apatite in bone tissue is lower than 1.67,[45] which is considered beneficial for instantaneous precipitation of bioequivalent apatite on its surface in vivo.[46] Conversely, stoichiometric apatite may require an induction time for precipitation. Therefore, the developed apatite-based nanomaterials with biomimetic features show a great potential for tissue engineering applications.

It is well recognized that excess and prolonged host inflammatory response could reprogram the cellular energy metabolism in periodontal tissue from oxidative phosphorylation to anaerobic glycolysis, leading to the occurrence of extracellular acidification.[47,48] Therefore, an acidic pH could serve as an external stimulus to control the release of anti-inflammatory agents for the regulation of cell behaviors via a self-modulatory mechanism under inflammatory conditions.[49,50] Figure 2F shows the drug release profiles of aspirin-laden nanocomposites at two different pH values: 5.5 and 7.4. Clearly, the release rate of aspirin from both ASA@tHALL and ASA@tHALLG was pH-sensitive. Compared to the neutral pH state, the release rate of aspirin from ASA@tHALL could be accelerated by an acidic pH. The different release profile may be ascribed to the difference in the swelling of the CMC/PLL self-assembly coating under neutral and acidic conditions. The coating may be more susceptible to swelling at acidic pHs than at a neutral pH.[51] Moreover, under a lower pH, the protonation of amino groups in the coatings most likely leads to the disintegration of the self-assembly multilayers, which may also contribute to the faster drug release rate.[52] A similar drug release profile was observed for the ASA@tHALLG nanocomposites. However, it was noted that the release rate of aspirin from the ASA@tHALLG nanocomposites was markedly lower compared to ASA@tHALL. It is suggested that the crosslinking of the CMC/PLL self-assembly by genipin could enhance the stability of the coatings by increasing the polymer density, eventually resulting in slower diffusion of aspirin through the coatings.[53] Due to its combined anti-inflammatory and pro-resolution effects, aspirin has been extensively explored for modulation of the host inflammatory response in periodontal disease.[54,55] However, traditional delivery strategies based on apatite nanomaterials may compromise aspirin's therapeutic effect, as it shows concentration- and time-dependent activity in the regeneration of periodontal tissue. Uncontrolled excess release of aspirin could actually inhibit osteogenesis, and the immobilized drug may have a limited effect on eventual tissue repair due to restricted access to the intracellular pharmacological target.[56–58] In our study, the coating designed on the surface of biomimetic nano apatite can not only be employed to encapsulate bioactive components but also control the release of drugs in a pH-responsive manner. Hence, it is believed that the developed biomimetic smart nanoplatform (ASA@tHALLG) could achieve site-specific and "on-demand" delivery of anti-inflammatory drugs based on host inflammatory response.

Cytocompatibility Evaluation of Biomimetic Smart Nanoplatform

Cytocompatibility is a prerequisite for the application of materials in the biomedical field.[59] Thus, indicators of cytocompatibility such as early cell adhesion behavior, cell growth, and LDH leakage of hPDLSCs exposed to ASA@tHALLG nanocomposites were systematically assessed in our study. Figure 3A and B shows the early adhesion of viable hPDLSCs when cocultured with different samples for 3 h using FDA staining. Clearly, compared to the tHA group, there were more adherent cells observed in the ASA@tHALLG group, as indicated by the green fluorescence, suggesting the positive effect of ASA@tHALLG on early cell adhesion, which was further revealed by SEM investigation at 24 h after incubation. As shown in Figure 3C, the cells showed a longitudinal morphology in all groups. Compared with bare tHA and its tHALLG counterpart, a better spreading shape with abundant cellular filopodia was observed in cells subjected to ASA@tHALLG nanocomposites. Further, the fluorescence images from F-actin staining (Figure 3D) indicated that hPDLSCs exposed to various nanocomposites showed spreading and filamentous morphology with direct cell-to-cell interactions. However, the optimal cell adhesion was displayed in the ASA@tHALLG group in comparison with the tHA group, which was indicated by the extended filopodia with visibly more mature F-actin intracellular stress fibers in the cells. One possible explanation is that bare tHA nanocomposites may trigger an inflammatory response to some extent in hPDLSCs,[60] but ASA@tHALLG could alleviate the foreign body response of cells by releasing aspirin, a non-steroidal anti-inflammatory drug with the capability of mitigating the exogenous pro-inflammatory stimuli from tHA.[61] It is well recognized that cell adhesion is the first step in initiating the normal performance of cellular functions. Thereby, the improved early cell adhesion behavior revealed by SEM and fluorescence observation implied that the delivery of aspirin via the GCP self-assembly may contribute to the capability of ASA@tHALLG to steer cellular behavior (eg, proliferation).

Figure 3E shows the results from the CCK-8 assay, which was used to evaluate the proliferation of hPDLSCs co-cultured with different samples for 1, 3, and 5 d. It can be seen that the hPDLSCs displayed a time-dependent proliferation in all test groups during the whole culture period, although the fastest cell growth was observed in the TCP control group. It is suggested that the tHA-based nanocomposites could support normal proliferation of hPDLSCs. However, it is noted that the lowest OD450 value was detected in the tHA group during incubation, indicating a negative impact of tHA on cell growth. A similar phenomenon was reported in previous studies, where nano apatite harbored a concentration-dependent cytotoxic effect on osteoblasts and human mesenchymal stem cells, which may be ascribed to the pro-inflammatory impact of nanomaterials on cells.[62,63] After surface functionalization, the inhibitory effect of tHA nanocomposite on cell growth was noticeably mitigated, especially in the ASA@tHALLG group, as indicated by a significantly enhanced OD450 value beginning at day 3. It is suggested that the ASA@tHALLG nanocomposites have great advantages in the proliferation of hPDLSCs over bare tHA.

LDH is an intracellular enzyme that can be released into culture medium when the integrity of the cell membrane is damaged.[64] Therefore, to further evaluate the cytocompatibility of the ASA@tHALLG nanocomposites, we performed an LDH assay after incubating the prepared samples with hPDLSCs for 24 h, as shown in Figure 3F. Obviously, compared to the control group, there was a significant increase in LDH leakage in the tHA group, indicating the negative impact of tHA on the integrity of plasma membranes. When the cells were cultured with ASA@tHALLG nanocomposites, the amount of released LDH markedly decreased, although there was no significant difference between the tHALLG and ASA@tHALLG groups, implying the low cytotoxic effect of ASA@tHALLG nanocomposites on hPDLSCs. Taken together, on the basis of studies regarding early cell adhesion behavior, cell growth, and LDH leakage, it can be concluded that ASA@tHALLG nanocomposites with enhanced cytocompatibility show great potential for application in the field of periodontal medicine.

Anti-Inflammatory Effect Analysis of Biomimetic Smart Nanoplatform

hPDLSCs play a crucial role in the reconstruction of periodontal tissue after regenerative therapy.[65,66] At early stages of tissue healing, a moderate inflammatory response could contribute to the in vivo performance of stem cells and benefit the regeneration of periodontal tissue. However, excessive and prolonged inflammatory response in hPDLSCs may cause accumulation of intracellular ROS, which are related to the oxidative damage to various biomolecules in cells, such as

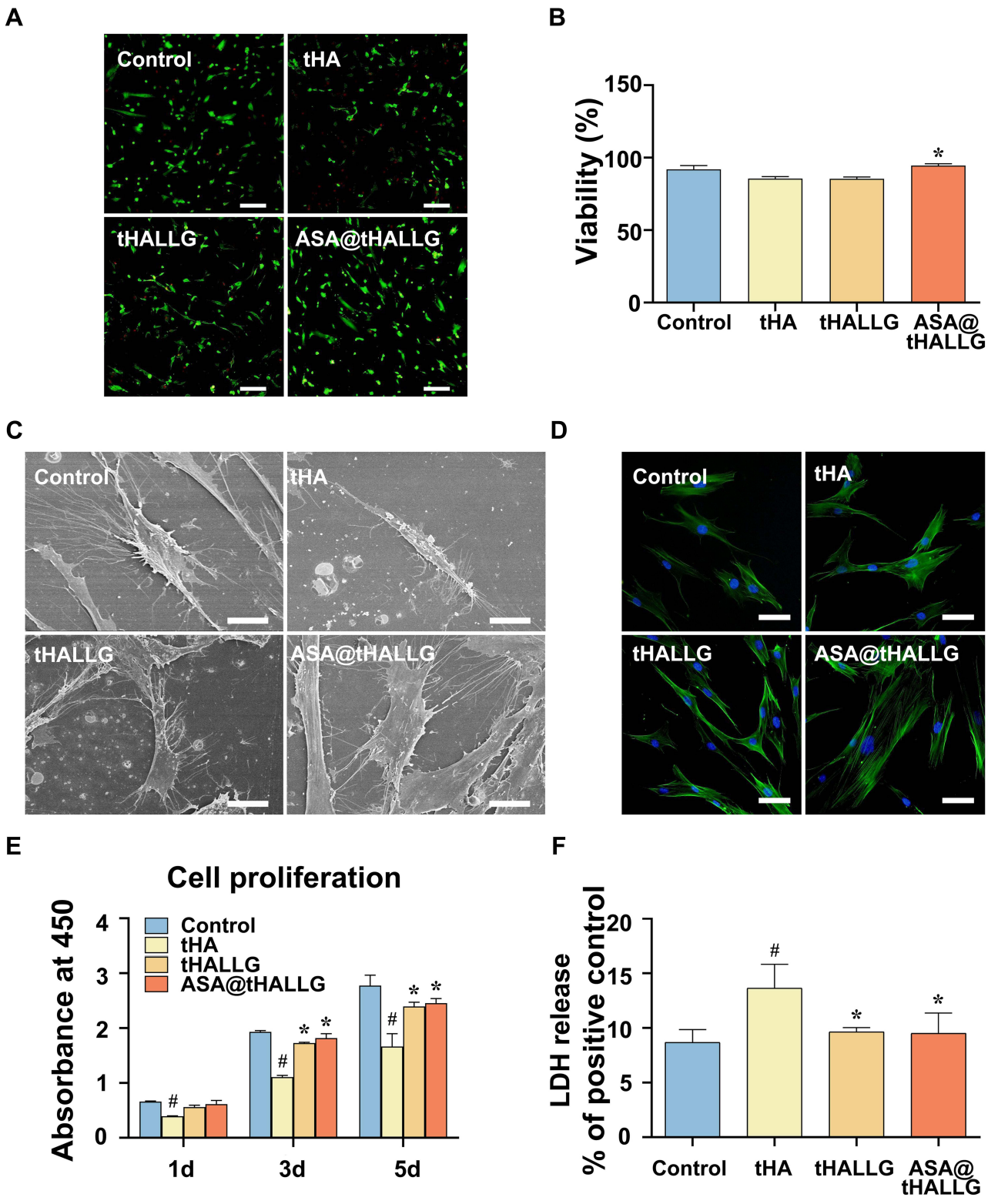

Figure 3 Cytocompatibility evaluation of synthesized biomimetic smart nanoplatform. (**A** and **B**) Staining and quantitative evaluation of viable hPDLSCs sub-cultured with tHA, tHALLG and ASA@tHALLG nanocomposites at 3 h after seeding. Scale bars = 200 μm. (**C**) SEM observation (Scale bars = 20 μm) and (**D**) cytoskeletal staining of hPDLSCs subjected to tHA, tHALLG and ASA@tHALLG nanocomposites. Scale bars = 50 μm. (**E**) The proliferation of hPDLSCs co-cultured with tHA, tHALLG and ASA@tHALLG nanocomposites. (**F**) LDH release of hPDLSCs subjected to tHA, tHALLG and ASA@tHALLG nanocomposites. #$p < 0.05$ compared to control group. *$p < 0.05$ compared to tHA group.

lipids, proteins, and DNA, eventually leading to the dysfunction of stem cells and in turn healing failure in periodontal tissue.[67,68] It is well known that aspirin is an FDA-approved drug that has been widely applied for the treatment of inflammatory diseases such as rheumatoid arthritis and fever caused by bacterial infection.[54] By inhibiting the synthesis and release of pro-inflammatory mediators, aspirin can mitigate the host inflammatory response to exogenous and endogenous stimuli.[69] In our study, the ASA@tHALLG nanocomposites showed pH-dependent aspirin-release behavior from the GCP assembly functionalized tHA composites. Therefore, to further investigate whether aspirin released from the ASA@tHALLG nanocomposites could maintain its bioactivity for regulation of the inflammatory response of hPDLSCs, we performed assays to evaluate pro-inflammatory cytokine gene expression and ROS generation in the hPDLSCs at 24 h after coculturing.

Figure 4A shows the gene expression of *TNF-α, IL-6*, and *IL-1β* in hPDLSCs exposed to different nanocomposites under LPS stimulation. *TNF-α* is a kind of major pro-inflammatory cytokine that can be produced by hPDLSCs in response to LPS and other bacterial products.[70] Excessive *TNF-α* release could trigger oxidative stress in stem cells, which is related to the impaired repair capacity of periodontal tissue.[71] *IL-6* is a multifunctional cytokine that serves as regulator of osteoclast recruitment and differentiation into mature osteoclasts.[72] *IL-1β*, a featured cytokine in periodontitis, is implicated in extracellular matrix degradation and periodontal tissue destruction via promoting the expression of collagenolytic enzymes and matrix metalloproteinases.[73] The gene expression analysis clearly showed that hPDLSCs

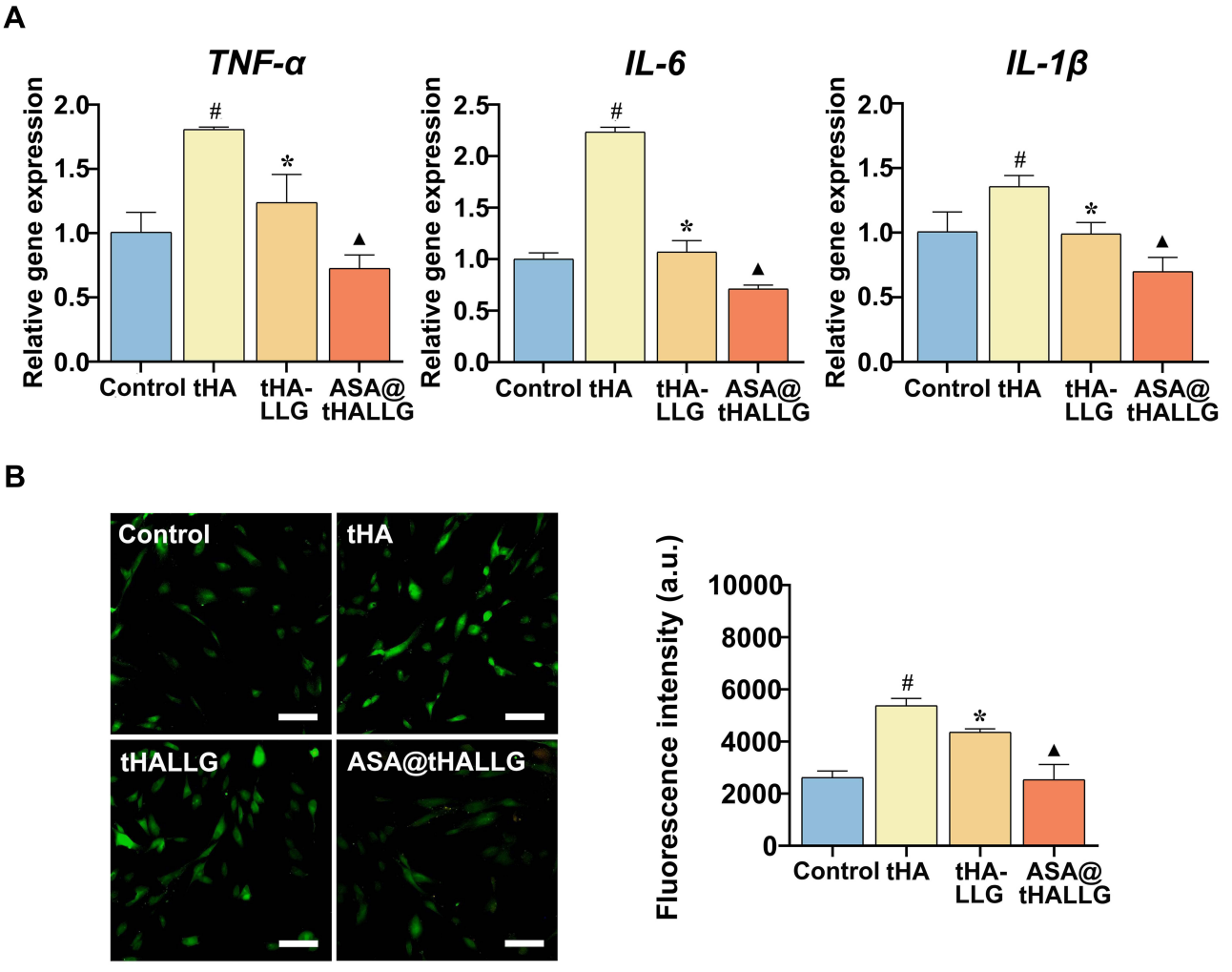

Figure 4 Anti-inflammatory effect analysis of biomimetic smart nanoplatform. (**A**) qPCR analysis of pro-inflammatory cytokine genes encoding *TNF-α, IL-6* and *IL-1β* in hPDLSCs co-cultured with tHA, tHALLG and ASA@tHALLG nanocomposites. (**B**) ROS production of hPDLSCs subjected to tHA, tHALLG and ASA@tHALLG nanocomposites. Scale bars = 100 μm. #$p < 0.05$ compared to control group. *$p < 0.05$ compared to tHA group. ▲$p < 0.05$ compared to tHALLG group.

from the tHA group showed higher mRNA expressions of *TNF-α, IL-6*, and *IL-1β* than those treated with LPS alone (control group), suggesting that tHA could amplify the inflammatory response of LPS-treated hPDLSCs. After incubation with the tHALLG nanocomposite, the hPDLSCs displayed a decreased expression of proinflammatory cytokines at the mRNA level, implying an anti-inflammatory effect of the GCP assembly on stem cells. It is noted that among all groups, the ASA@tHALLG group showed the highest down-regulation of proinflammatory cytokine gene expression. These results indicate that the aspirin released from ASA@tHALLG effectively repressed the inflammatory response of hPDLSCs to nanomaterials and bacterial product, which was further confirmed by the ROS assay. As shown in Figure 4B, ROS production in hPDLSCs was significantly increased in the tHA group compared to the control group, which may be ascribed to the pro-inflammatory effect of nano apatite on hPDLSCs. Due to coating the GCP assembly onto the surface of tHA, a decrease in ROS level was detected in the tHALLG group, which was accompanied by the anti-inflammatory activity of the GCP assembly, as already described. It is suggested that the GCP assembly may ameliorate oxidative stress in stem cells via inhibiting their inflammatory response. The intensity of ROS generation was further markedly decreased in the ASA@tHALLG group, highlighting the anti-inflammatory effect of the released aspirin on the tHA-induced oxidative stress response in hPDLSCs. Overall, the evaluations of pro-inflammatory cytokine gene expression and ROS production in hPDLSCs indicated that the encapsulation process via the GCP assembly did not alter the bioactivity of aspirin. The pH-responsive release of aspirin from the GCP assembly was able to not only endow tHA nanocomposite with enhanced anti-inflammatory effect but also mitigate oxidative stress in hPDLSCs induced by pro-inflammatory stimuli.

Antibacterial Activity Evaluation of Biomimetic Smart Nanoplatform

Pathogenesis of infection, the main source of exogenous pro-inflammatory stimulus, is considered to be one of the major reasons for the failure of periodontal regeneration therapy.[74] It is well known that the colonization of bacteria at the interface between graft materials and surrounding periodontal tissue is the first critical step in the pathogenesis of infection. Thus, preventing bacterial adhesion and proliferation near implanted materials at the early postoperative period is critical for an optimal regenerative outcome in periodontal tissue. Compared to the major pathogen in the progression of adult periodontitis and peri-implantitis like *Porphyromonas gingivalis* (*P. gingivalis*),[75] the common pathogenic bacteria in oral cavity such as Gram-negative *Escherichia coli* (*E. coli*) and Gram-positive *Staphylococcus aureus* (*S. aureus*) have been reported to impose a higher risk of post-surgical infection at early stage after implantation of graft materials.[76,77] Therefore, to assess the antibacterial activity of the functionalized tHA nanocomposites, the initial adhesion and growth of *E. coli* (Gram-negative) and *S. aureus* (Gram-positive) were investigated after exposure to different samples over a fixed time. Figure 5A shows the amount of *E. coli* and *S. aureus* in different groups. At the initial adhesion stage (4 h), the tHA group showed fewer *E. coli* and *S. aureus* than the control group, which was ascribed to the antifouling property of pDA layers on the tHA surface.[78] In the tHALLG and ASA@tHALLG groups, the early colonizing bacteria were further decreased compared to the tHA group. In the proliferation phase (24 h), the OD values of two different bacteria in the control group increased as time progressed. However, compared to the control group, the number of adherent bacteria was dramatically decreased in the functionalized tHA nanocomposites, which was further confirmed by fluorescent staining of viable bacteria (Figure 5B). Specifically, after 24 h of incubation, the tHALLG group showed a 44% reduction and the ASA@tHALLG group showed a 39% reduction in *E. coli* adhesion compared to the control group. In the case of *S. aureus*, a similar efficacy was observed in reducing the number of adherent bacteria by the ASA@tHALLG and tHALLG nanocomposites. These results indicated that GCP assembly coated on the surface of tHA nanocomposite could effectively inhibit the adhesion and proliferation of *E. coli* and *S. aureus*. Moreover, it was observed in SEM images (Figure 5C) that, different from a uniform rod-like *E. coli* and spherical-like *S. aureus* in the control group, both adherent bacteria showed an irregular shape with crumpling features or cell rupture in each nanocomposite group. It is well known that CMC and PLL have a broad antibacterial spectrum, which includes both gram-negative and gram-positive bacteria.[79,80] Via electrostatic interaction, these components in GCP may disrupt the cell wall and membrane integrity of bacteria.[81] Moreover, PLL also has the ability to directly restrain the central carbon metabolism in bacteria.[82] Therefore, our findings suggested that the inhibitory effect of the ASA@tHALLG nanocomposite on bacteria growth may be enabled through contact-killing mode.

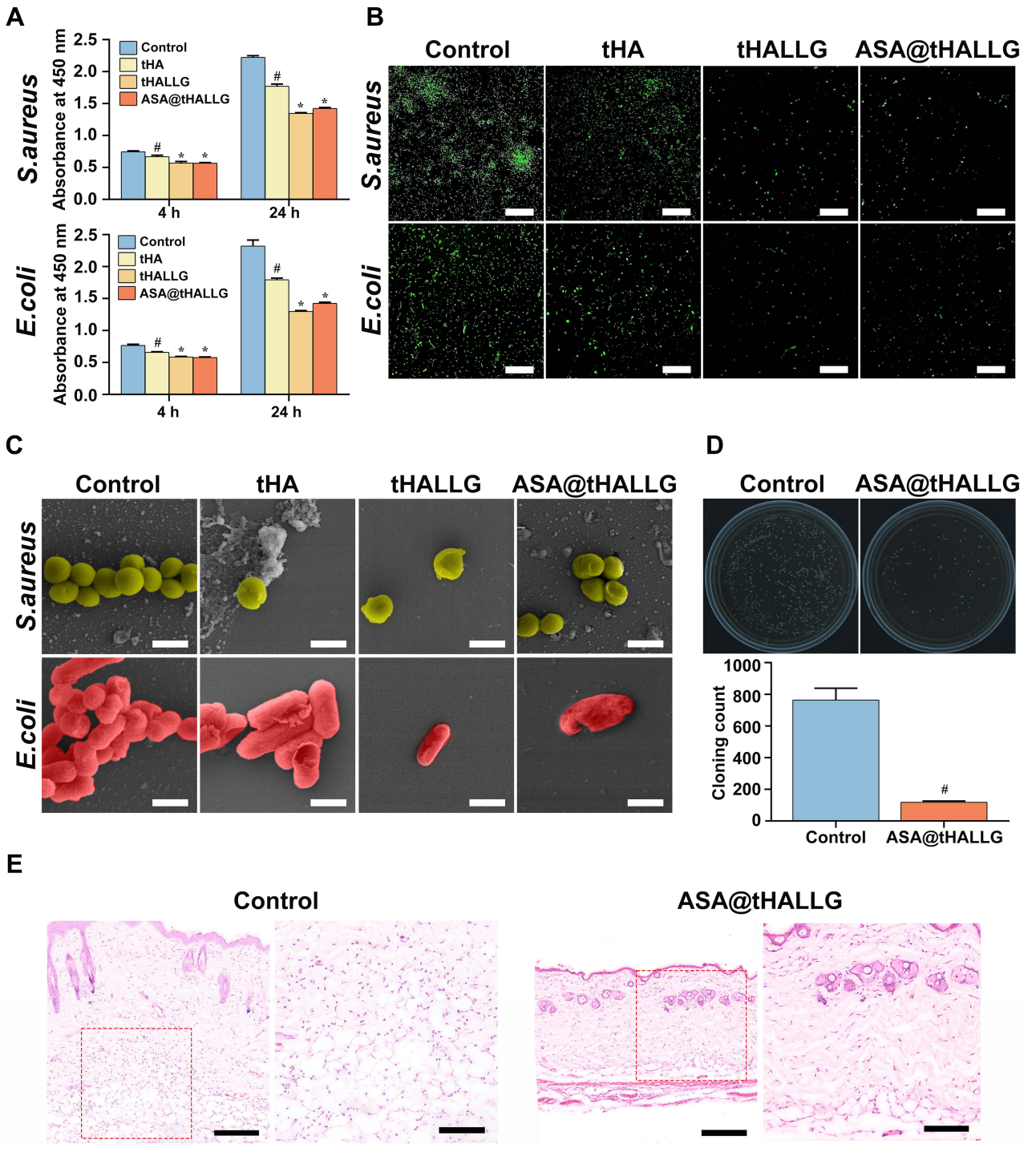

Figure 5 Antibacterial activity evaluation of biomimetic smart nanoplatform. (**A**) Antibacterial activities of different nanocomposites against *E. coli* and *S. aureus* cultured for 4 and 24 h. (**B**) Fluorescent staining of adherent *E. coli* and *S. aureus* at 24 h after incubation with different nanocomposites. Scale bars = 50 μm. (**C**) SEM images of the morphology and number of adherent *E. coli* and *S. aureus* after incubation with different nanocomposites. Scale bars = 1 μm. (**D**) Typical images and quantitative analysis of bacterial colony-forming units obtained from subcutaneous tissue fluid. (**E**) H&E staining images of mouse subcutaneous tissue. The region outlined by the red box are shown on the right. #$p < 0.05$ compared to control group. *$p < 0.05$ compared to tHA group.

To further assess in vivo antibacterial activity, the ASA@tHALLG nanocomposites were subcutaneously implanted into mice. Live bacterial colonies collected from tissue fluid were counted, as shown in Figure 5D. Compared to the control group, the number of bacterial colonies significantly decreased from 764.5 ± 64.2 to 119 ± 6.4 in the ASA@tHALLG group, suggesting the excellent antibacterial activity of the ASA@tHALLG nanocomposites, which

agreed with the results of the in vitro study. Furthermore, less infiltration of inflammatory cells was observed in the soft tissue around implants from the ASA@tHALLG group according to a histological analysis (Figure 5E). These findings indicated that the GCP assembly functionalized tHA nanocomposite with enhanced antibacterial activity may be beneficial for the reduction of exogenous pro-inflammatory stimuli from bacterial infection.

Osteogenic Activity Evaluation of Biomimetic Smart Nanoplatform

For periodontal tissue repair, osteogenic differentiation of hPDLSCs around graft materials is a critical event during healing. Among various osteogenic indicators, ALP is an early hallmark that is widely used to assess the osteogenic potential of stem cells.[83] Thus, the ALP activity of hPDLSCs cocultured with tHA, tHALLG, and ASA@tHALLG nanocomposites was measured on day 7, as depicted in Figure 6A. Clearly, the hPDLSCs in the tHA group showed a higher ALP activity than those in the control group, suggesting that the tHA nanocomposite could induce the osteogenic differentiation of stem cells. Moreover, ALP was elevated in the tHALLG group due to the surface functionalization of the GCP assembly on the tHA nanocomposite. This finding indicated that the GCP assembly surface coating on tHA could promote ALP expression in hPDLSCs, which is regarded as the first checkpoint for osteogenic differentiation. Notably, ALP activity in cells from the ASA@tHALLG group was approximately 1.4 times greater than that of the tHALLG group, highlighting the impact of aspirin released from ASA@tHALLG nanocomposite on the ALP production of hPDLSCs. These results were further verified by an ALP staining assay.

Calcium deposition is a late-stage marker for the osteogenic differentiation of hPDLSCs.[84] Due to its bone-like structures, the inorganic calcium produced by stem cells plays an imperative role during the reconstruction of periodontal tissue. To assess the mineralization efficiency of hPDLSCs subjected to prepared samples, an ARS staining analysis was performed after incubation for 21 days, as shown in Figure 6B. The difference in calcium deposition among groups displayed a similar trend to the changes in ALP activity. It was clearly observed that compared to the control group, the tHA, tHALLG, and ASA@tHALLG groups showed a considerable increase in the formation of calcium nodules. Particularly, the most intensive and extensive area of calcium nodules was found in the ASA@tHALLG group. Taken together, ALP and ARS staining assays demonstrated that local delivery of aspirin from the ASA@tHALLG nanocomposite could facilitate the osteogenic differentiation of hPDLSCs.

The initiation and completion of osteogenic differentiation are regulated by a cascade of signal transduction events. An in-depth study at the transcriptional level is beneficial for interpreting the cellular response to nanocomposites.[85] Thereby, the expression of osteogenic genes encoding RUNX2, ALP, and COL1A1 was measured by qPCR experiments on day 7 (Figure 6C). As expected, the expression of RUNX2, ALP, and COL1A1 in hPDLSCs co-cultured with tHA, tHALLG, and ASA@tHALLG nanocomposites was enhanced compared to the control group. However, the highest mRNA level of osteo-specific markers was shown in cells from the ASA@tHALLG group. RUNX2 is the most upstream transcription factor essential for osteoblast differentiation and chondrocytes, and it could activate the transcription of other osteogenic markers such as ALP and COL1A1 (a marker encoding the major bone matrix protein) via binding to their promoter regulatory domain.[86] Therefore, the gene expression analysis demonstrated the effect of aspirin on the osteogenic differentiation of stem cells, which was also proved by the immunofluorescent staining of osteogenic-associated markers RUNX2 and OPN (Figure 6D). Taken together, our data suggested that the aspirin-loaded GCP assembly could endow tHA with a favorable bioactivity for the osteogenesis of hPDLSCs.

In vivo Experiment

Encouraged by the results from the in vitro experiments, the in vivo effect of the ASA@tHALLG nanocomposite on the repair of periodontal tissue during healing was further investigated for future clinical translational applications. To this end, we established a tooth root fenestration preclinical model on the buccal plates of a rat mandible as previously described,[32] and then applied the prepared nanocomposites to the defects (Figure 7A). At four weeks after surgery, specimens were harvested and processed for μCT analysis. Figure 7B shows 3D reconstructed CT images of the defects in the region of interest (ROI) coupled with a corresponding quantitative analysis of bone volume as a ratio of tissue volume (BV/TV). Obviously, the regeneration of periodontal bone tissue at bone–ligament interfaces was boosted in the tHA and tHALLG treatment groups, as indicated by an increased value of BV/TV compared to the control group ($p <$

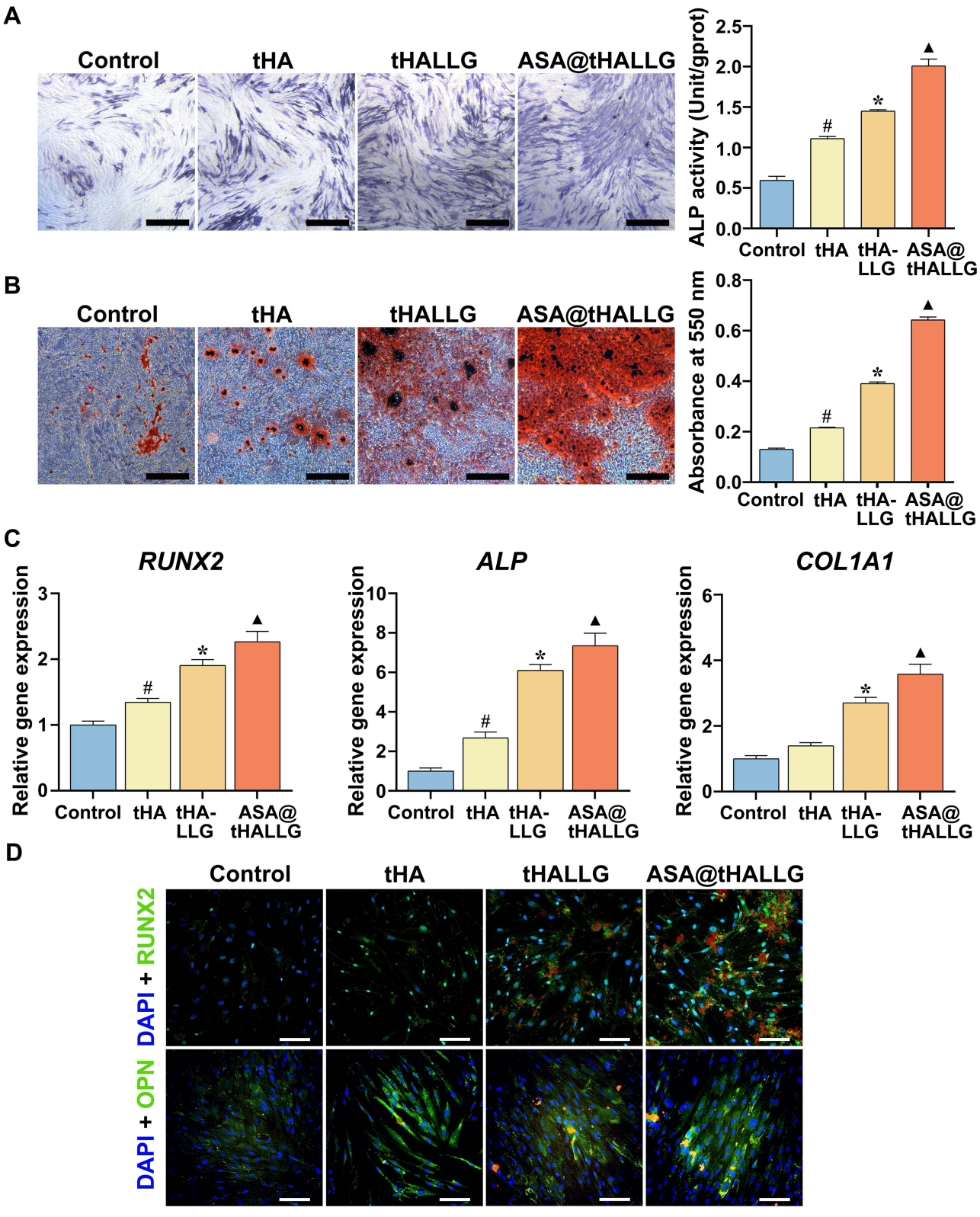

Figure 6 Osteogenic differentiation of hPDLSCs co-cultured with tHA, tHALLG and ASA@tHALLG nanocomposites. (**A**) Representative photographs of ALP staining and ALP activity measurement. Scale bars = 500 μm. (**B**) Representative photographs of ARS staining and quantification of ARS for calcium deposition. Scale bars = 500 μm. (**C**) qPCR analysis of the osteogenic genes encoding ALP, RUNX2 and COL1A1. (**D**) Representative immunofluorescent staining of osteogenic proteins RUNX2 and OPN. Scale bars = 100 μm. #$p < 0.05$ compared to control group. *$p < 0.05$ compared to tHA group. ▲$p < 0.05$ compared to tHALLG group.

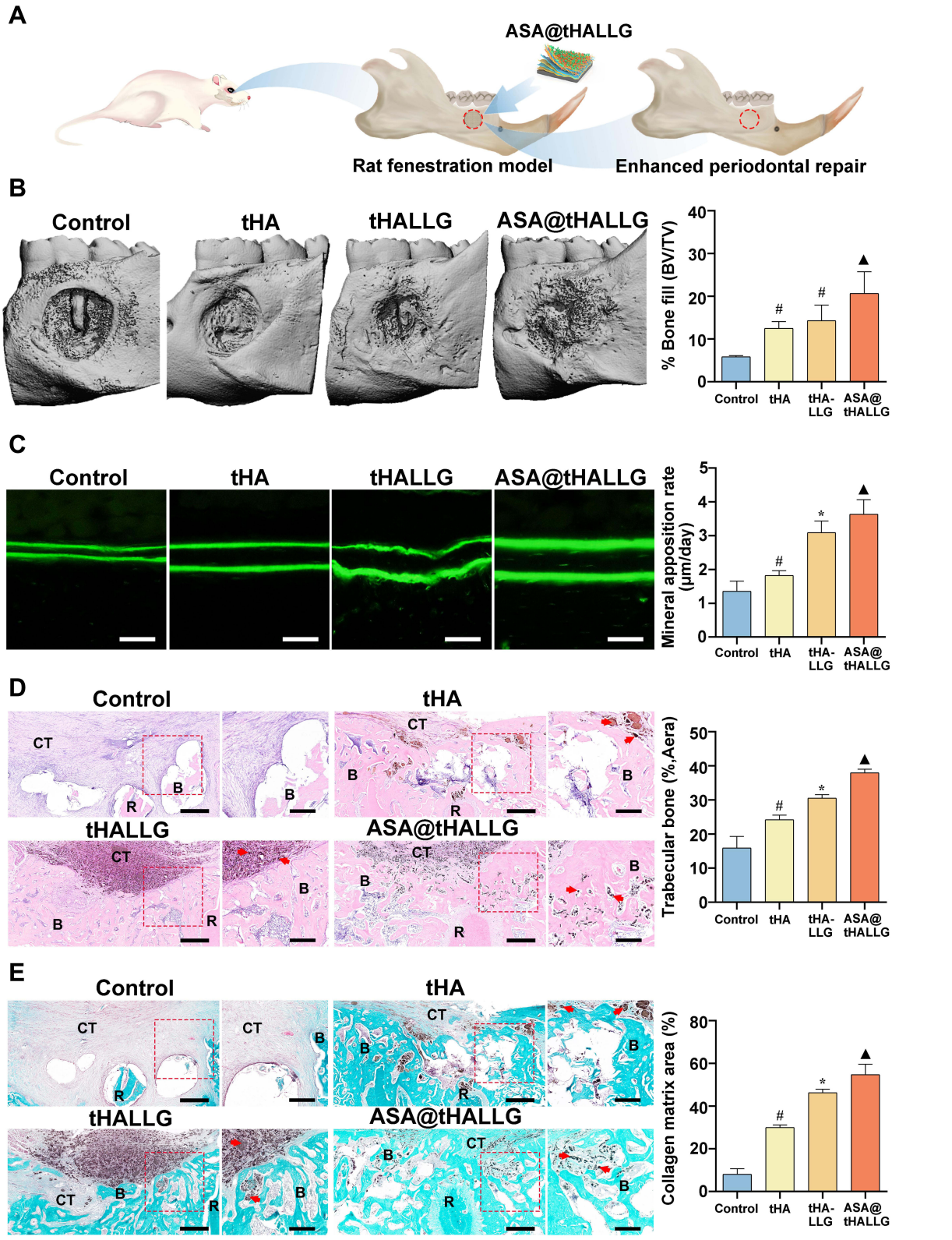

Figure 7 Biomimetic smart nanoplatform promotes regeneration of periodontal bone tissue in vivo. (**A**) Establishment of rat fenestration model for implantation of nanomaterials prepared in our study. (**B**) μCT images and analysis of 3D-reconstructed models showing the periodontal bone formation in the region of interest at 4 weeks post-operation. (**C**) Sequential fluorescent labelling observation showing the growth rate of newly formed periodontal bone tissue. (**D**) H&E staining and quantification of newly formed periodontal bone tissue in the periodontal defects. (**E**) Masson-trichrome staining and quantification of newly formed collagen matrix in the periodontal defects. #$p < 0.05$ compared to control group. *$p < 0.05$ compared to tHA group. ▲$p < 0.05$ compared to tHALLG group.
Abbreviations: B, bone; R, the root of the tooth; CT, connective tissues.

0.05), suggesting the osteoinductive potential of tHA and tHALLG nanocomposites in vivo as well. It is noteworthy that corresponding to the findings from in vitro osteogenic activity evaluation (Figure 6), tHALLG group showed more regenerated bone tissues than tHA group. It may be due to the positive effect of GCP assembly on the regulation of inflammatory response (Figure 4). Moreover, the scavenging ability of free radicals by the active hydroxyl and amino groups in GCP assembly may also contribute to the enhanced osteogenesis via alleviation of oxidative stress in PDLSCs under inflammatory condition.[87–89] However, the most nascent bone tissue was detected in defects from the ASA@tHALLG group, which may be attributed to the extra effect of aspirin released from the GCP assembly. The data from the μCT analysis were further confirmed by fluorochrome labeling to evaluate the time-dependent bone formation (Figure 7C). Obviously, an enhancement of the growth rate of the mineralization among the control, tHA, and tHALLG groups was detected. With the encapsulation of aspirin into the GCP assembly, the mineral deposition rate was further increased, which corresponded to the improved growth and osteogenic differentiation of hPDLSCs in the ASA@tHALLG group observed from in vitro assays, providing additional in vivo evidence for the contribution of aspirin to periodontal bone regeneration.

To further identify the composition of regenerated tissue at the defect sites, the newly formed tissues were analyzed by histological staining. As shown in the results from H&E staining (Figure 7D), the defects were mainly filled with fibrous tissues in the control group at four weeks after surgery. In contrast, obvious bone-like and microvascular structures were detected in the defects implanted with apatite nanocomposites, which were also revealed in Masson's trichrome staining assay (Figure 7E). Masson's trichrome staining is a selective histological approach for evaluating collagen type I, which constitutes the major organic component in bone-specific matrix. Clearly, the control group showed limited bone-specific collagen in the defects (approximately 8%). However, the newly-formed collagen type I content was significantly increased in defects implanted with ASA@tHALLG nanocomposite. Moreover, immunohistochemical staining showed that the region implanted with ASA@tHALLG nanocomposite expressed the highest production of osteogenic proteins, OPN, and OCN, among all groups (Figure S2). OCN is a bone-specific matrix protein that is mainly produced by osteoblasts. It plays an imperative role in the initiation of hydroxyapatite crystal formation during the mineralization of bone matrix.[90] OPN is a marker for osteoblasts at an intermediate stage of osteogenesis, which is involved in the synthesis of the organic matrix.[91] Previous studies reported that local delivery of aspirin via a scaffold could upregulate osteogenic proteins and the mineralization of stem cells under inflammatory conditions.[92,93] Accordingly, as expected, after implantation of ASA@tHALLG nanocomposites into defects, the released aspirin from the GCP assembly enhanced the osteogenic potential of hPDLSCs at bone-ligament interfaces, eventually leading to an accelerated remodeling of periodontal bone tissue. Moreover, it is noted that due to the anti-inflammatory activity of aspirin, the host inflammatory response was markedly inhibited during the healing process of the defects treated with ASA@tHALLG nanocomposites, as indicated by the significantly reduced positive staining areas of TNF-α and IL-1β (Figure S3) in the defect regions. A similar finding was reported in a previous study, where a thermosensitive hydrogel loaded with aspirin showed effective inhibition against pro-inflammatory response in periodontium.[94] Recently, increasing evidence demonstrated that excessive and prolonged host inflammatory response is one of the major risk factors for failure of periodontal regenerative therapy,[11,95,96] which may be ascribed to the overexpression of pro-inflammatory cytokines in periodontal tissue.[67,97] Via binding to their receptors, these cytokines could induce nuclear translocation and accumulation of nuclear factor kappa B (NF-κB) in PDLSCs.[67,98] Moreover, oxidative stress induced by pro-inflammatory cytokines is also implicated in the activation of NF-κB.[99,100] As a master regulator of inflammation, NF-κB-mediated signaling pathway has been reported to have crosstalk with Wnt/catenin pathway,[67,101] which plays a pivotal role during osteogenic differentiation of stem cells.[67,101,102] Cun-Yu Wang et al previously proved that activation of NF-κB can inhibit osteogenic differentiation of stem cells by promoting β-catenin degradation.[98] Based on above inflammation mediated regulatory mechanism, aspirin released from ASA@tHALLG nanocomposites may interfere NF-κB signaling pathway through inhibition of inflammatory response,[57,92] in turn enhancing Wnt-dependent osteogenic commitment of PDLSCs, the critical cells responsible for regeneration of periodontal tissue, in inflammatory microenvironment.[67,103] Therefore, in agreement with the in vitro experiments, the results obtained from the in vivo studies demonstrated that the ASA@tHALLG nanocomposites possessed an excellent capacity to facilitate the reconstruction of periodontal bone tissue, with great potential for applications in periodontal and bone tissue engineering.

However, it should be pointed out that owing to the limitation of defect size and technical challenges,[32,104] it is difficult to accurately evaluate the effect of graft materials on the regeneration of periodontal attachment including periodontal ligament and cementum using rat fenestration model presented in our study.[32,104] Therefore, large animal models such as canine and swine are needed for further in vivo validation of ASA@tHALLG nanocomposites targeting periodontal regeneration in the future.[105–107]

Conclusion

The pathological microenvironment, driven by an excessive and prolonged host inflammatory response to various detrimental stimuli such as foreign body reaction and microbial infection, is a hindrance for the reconstruction of periodontal tissue defects. To address this issue, a multifunctional nanoplatform was developed as graft materials in this work by constructing an inflammatory-responsive coating on a biomimetic apatite nanocomposite, which could release an anti-inflammatory agent through a pH-sensitive mechanism. Our study demonstrated the stimuli-responsive profile of an engineered "building block" on the apatite nanocomposite towards improving regeneration of periodontal tissue via inhibiting the host inflammatory response to implants and infection, which is beneficial for the elimination of accumulated ROS in hPDLSCs. Additionally, the engineered bioactive apatite nanocomposite was shown to be able to reduce exogenous pro-inflammatory stimuli due to its noticeable antibacterial activity against common periodontal pathogens. The present study offers a facile, environmentally friendly, and cost-effective approach for the synthesis of a biomimetic smart nanoplatform with pH-responsive anti-inflammatory effect, which has great potential in the field of periodontal and orthopedic regenerative medicine.

Acknowledgments

This work was supported in part by the Chongqing Postdoctoral Science Foundation (X11229), the Postdoctoral Fund Project of the Chongqing Natural Science Foundation (cstc2021jcyj-bshX0101), and Program for Youth Innovation in Future Medicine, Chongqing Medical University (W0055).

Disclosure

The authors report no conflicts of interest in this work.

References

1. Janakiram C, Dye BA. A public health approach for prevention of periodontal disease. *Periodontol*. 2020;84(1):202–214. doi:10.1111/prd.12337
2. Righolt AJ, Jevdjevic M, Marcenes W, Listl S. Global-, regional-, and country-level economic impacts of dental diseases in 2015. *J Dent Res*. 2018;97(5):501–507. doi:10.1177/0022034517750572
3. Kinane DF, Stathopoulou PG, Papapanou PN. Periodontal diseases. *Nat Rev Dis Primers*. 2017;3:17038. doi:10.1038/nrdp.2017.38
4. Benic GI, Bienz SP, Song YW, et al. Randomized controlled clinical trial comparing guided bone regeneration of peri-implant defects with soft-type block versus particulate bone substitutes: six-month results of hard-tissue changes. *J Clin Periodontol*. 2022;49(5):480–495. doi:10.1111/jcpe.13606
5. Ou Q, Huang K, Fu C, et al. Nanosilver-incorporated halloysite nanotubes/gelatin methacrylate hybrid hydrogel with osteoimmunomodulatory and antibacterial activity for bone regeneration. *Chem Eng J*. 2020;382:123019. doi:10.1016/j.cej.2019.123019
6. Montero E, Roccuzzo A, Molina A, Monje A, Herrera D, Roccuzzo M. Minimal invasiveness in the reconstructive treatment of peri-implantitis defects. *Periodontol*. 2022;00:1–18.
7. Passanezi E, Sant'Ana ACP. Role of occlusion in periodontal disease. *Periodontol*. 2019;79(1):129–150. doi:10.1111/prd.12251
8. Woo HN, Cho YJ, Tarafder S, Lee CH. The recent advances in scaffolds for integrated periodontal regeneration. *Bioact Mater*. 2021;6(10):3328–3342. doi:10.1016/j.bioactmat.2021.03.012
9. Hajishengallis G, Chavakis T, Lambris JD. Current understanding of periodontal disease pathogenesis and targets for host-modulation therapy. *Periodontol*. 2020;84(1):14–34. doi:10.1111/prd.12331
10. Gruber R. Osteoimmunology: inflammatory osteolysis and regeneration of the alveolar bone. *J Clin Periodontol*. 2019;46:52–69. doi:10.1111/jcpe.13056
11. Wang B, Shao J, Fu J, et al. Topical host-modulating therapy for periodontal regeneration: a systematic review and meta-analysis. *Tissue Eng Part B-Rev*. 2019;25(6):526–543. doi:10.1089/ten.teb.2019.0184
12. Kaplani K, Koutsi S, Armenis V, et al. Wound healing related agents: ongoing research and perspectives. *Adv Drug Deliv Rev*. 2018;129:242–253. doi:10.1016/j.addr.2018.02.007
13. Villarreal-Leal RA, Healey GD, Corradetti B. Biomimetic immunomodulation strategies for effective tissue repair and restoration. *Adv Drug Deliv Rev*. 2021;179:113913. doi:10.1016/j.addr.2021.113913

14. Wang M, Xie J, Wang C, Zhong D, Xie L, Fang H. Immunomodulatory properties of stem cells in periodontitis: current status and future prospective. *Stem Cells Int*. 2020;2020:9836518. doi:10.1155/2020/9836518
15. Slots J. Periodontitis: facts, fallacies and the future. *Periodontol*. 2017;75(1):7–23. doi:10.1111/prd.12221
16. Raziyeva K, Kim Y, Zharkinbekov Z, Kassymbek K, Jimi S, Saparov A. Immunology of acute and chronic wound healing. *Biomolecules*. 2021;11(5):700. doi:10.3390/biom11050700
17. Neurath MF. Resolution of inflammation: from basic concepts to clinical application. *Semin Immunopathol*. 2019;41(6):627–631. doi:10.1007/s00281-019-00771-2
18. Zhuang Z, Yoshizawa-Smith S, Glowacki A, et al. Induction of M2 macrophages prevents bone loss in murine periodontitis models. *J Dent Res*. 2019;98(2):200–208. doi:10.1177/0022034518805984
19. Rossi JF, Lu ZY, Massart C, Levon K. Dynamic immune/inflammation precision medicine: the good and the bad inflammation in infection and cancer. *Front Immunol*. 2021;12:595722. doi:10.3389/fimmu.2021.595722
20. Sczepanik FSC, Grossi ML, Casati M, et al. Periodontitis is an inflammatory disease of oxidative stress: we should treat it that way. *Periodontol*. 2020;84(1):45–68. doi:10.1111/prd.12342
21. Zhang K, Wang S, Zhou C, et al. Advanced smart biomaterials and constructs for hard tissue engineering and regeneration. *Bone Res*. 2018;6:31. doi:10.1038/s41413-018-0032-9
22. Yang X, Zhang C, Deng D, Gu Y, Wang H, Zhong Q. Multiple stimuli-responsive MXene-based hydrogel as intelligent drug delivery carriers for deep chronic wound healing. *Small*. 2022;18(5):e2104368. doi:10.1002/smll.202104368
23. Boller LA, Shiels SM, Florian DC, et al. Effects of nanocrystalline hydroxyapatite concentration and skeletal site on bone and cartilage formation in rats. *Acta Biomater*. 2021;130:485–496. doi:10.1016/j.actbio.2021.05.056
24. Heidari G, Hassanpour M, Nejaddehbashi F, et al. Biosynthesized nanomaterials with antioxidant and antimicrobial properties. *Mater Chem Horizons*. 2022;1(1):35–48.
25. Beğiç N, Bener M, Apak R. Development of a green synthesized silver nanoparticle-based antioxidant capacity method using carob extract. *J Nanostructure Chem*. 2021;11(3):381–394. doi:10.1007/s40097-020-00374-6
26. Collins MN, Ren G, Young K, Pina S, Reis RL, Oliveira JM. Scaffold fabrication technologies and structure/function properties in bone tissue engineering. *Adv Funct Mater*. 2021;31(21):2010609. doi:10.1002/adfm.202010609
27. Mondal S, Dorozhkin SV, Pal U. Recent progress on fabrication and drug delivery applications of nanostructured hydroxyapatite. *Wiley Interdiscip Rev Nanomed Nanobiotechnol*. 2018;10(4):e1504. doi:10.1002/wnan.1504
28. Epple M. Review of potential health risks associated with nanoscopic calcium phosphate. *Acta Biomater*. 2018;77:1–14. doi:10.1016/j.actbio.2018.07.036
29. Lara-Ochoa S, Ortega-Lara W, Guerrero-Beltrán CE. Hydroxyapatite nanoparticles in drug delivery: physicochemistry and applications. *Pharmaceutics*. 2021;13(10):1642. doi:10.3390/pharmaceutics13101642
30. Gao X, Song J, Ji P, et al. Polydopamine-templated hydroxyapatite reinforced polycaprolactone composite nanofibers with enhanced cytocompatibility and osteogenesis for bone tissue engineering. *ACS Appl Mater Interfaces*. 2016;8(5):3499–3515. doi:10.1021/acsami.5b12413
31. Dararatana N, Seidi F, Hamel J, Crespy D. Controlling release kinetics of pH-responsive polymer nanoparticles. *Polym Chem*. 2020;11(10):1752–1762. doi:10.1039/C9PY01946D
32. Padial-Molina M, Rodriguez JC, Volk SL, Rios HF. Standardized in vivo model for studying novel regenerative approaches for multitissue bone-ligament interfaces. *Nat Protoc*. 2015;10(7):1038–1049. doi:10.1038/nprot.2015.063
33. Li Z, Pan W, Shi E, et al. A multifunctional nanosystem based on bacterial cell-penetrating photosensitizer for fighting periodontitis via combining photodynamic and antibiotic therapies. *ACS Biomater Sci Eng*. 2021;7(2):772–786. doi:10.1021/acsbiomaterials.0c01638
34. Xu X, Li Y, Wang L, et al. Triple-functional polyetheretherketone surface with enhanced bacteriostasis and anti-inflammatory and osseointegrative properties for implant application. *Biomaterials*. 2019;212:98–114. doi:10.1016/j.biomaterials.2019.05.014
35. Lyu Q, Hsueh N, Chai CLL. The chemistry of bioinspired catechol(amine)-based coatings. *ACS Biomater Sci Eng*. 2019;5(6):2708–2724. doi:10.1021/acsbiomaterials.9b00281
36. Richardson JJ, Björnmalm M, Caruso F. Multilayer assembly. Technology-driven layer-by-layer assembly of nanofilms. *Science*. 2015;348(6233):aaa2491. doi:10.1126/science.aaa2491
37. Liu Y, Cai Z, Sheng L, Ma M, Xu Q, Jin Y. Structure-property of crosslinked chitosan/silica composite films modified by genipin and glutaraldehyde under alkaline conditions. *Carbohydr Polym*. 2019;215:348–357. doi:10.1016/j.carbpol.2019.04.001
38. Liu Y, Luo D, Wang T. Hierarchical structures of bone and bioinspired bone tissue engineering. *Small*. 2016;12(34):4611–4632. doi:10.1002/smll.201600626
39. Ryu J, Ku SH, Lee H, Park CB. Mussel-inspired polydopamine coating as a universal route to hydroxyapatite crystallization. *Adv Funct Mater*. 2010;20(13):2132–2139. doi:10.1002/adfm.200902347
40. Mehdizadeh P, Orooji Y, Amiri O, Salavati-Niasari M, Moayedi H. Green synthesis using cherry and orange juice and characterization of TbFeO3 ceramic nanostructures and their application as photocatalysts under UV light for removal of organic dyes in water. *J Clean Prod*. 2020;252:119765. doi:10.1016/j.jclepro.2019.119765
41. Abdullah OGH, Hanna RR, Salman YAK. Structural and electrical conductivity of CH:MC bio-poly-blend films: optimize the perfect composition of the blend system. *Bull Mat Sci*. 2019;42(2):64. doi:10.1007/s12034-019-1742-3
42. Wang D, Li J, Zhang L, Jiang C, Yang P, Cheng X. Synthesis and effect of highly active nano-SiO2 on ion/water transmission property of cement-based materials. *J Building Eng*. 2022;59:105054. doi:10.1016/j.jobe.2022.105054
43. Tryba AM, Krok-Borkowicz M, Kula M, et al. Surface functionalization of poly(l-lactide-co-glycolide) membranes with RGD-grafted poly(2-oxazoline) for periodontal tissue engineering. *J Funct Biomater*. 2022;13(1):4. doi:10.3390/jfb13010004
44. Vargas-Becerril N, Sánchez-Téllez DA, Zarazúa-Villalobos L, et al. Structure of biomimetic apatite grown on hydroxyapatite (HA). *Ceram Int*. 2020;46(18):28806–28813. doi:10.1016/j.ceramint.2020.08.044
45. Zhang L, Lu T, He F, et al. Physicochemical and cytological properties of poorly crystalline calcium-deficient hydroxyapatite with different Ca/P ratios. *Ceram Int*. 2022;48(17):24765–24776. doi:10.1016/j.ceramint.2022.05.126

46. Xiang M, Zhu M, Yang Z, et al. Dual-functionalized apatite nanocomposites with enhanced cytocompatibility and osteogenesis for periodontal bone regeneration. *ACS Biomater Sci Eng*. 2020;6(3):1704–1714. doi:10.1021/acsbiomaterials.9b01893
47. Gaber T, Strehl C, Buttgereit F. Metabolic regulation of inflammation. *Nat Rev Rheumatol*. 2017;13(5):267–279. doi:10.1038/nrrheum.2017.37
48. Wang L, Li Y, Ren M, et al. pH and lipase-responsive nanocarrier-mediated dual drug delivery system to treat periodontitis in diabetic rats. *Bioact Mater*. 2022;18:254–266. doi:10.1016/j.bioactmat.2022.02.008
49. Zhang CY, Gao J, Wang Z. Bioresponsive nanoparticles targeted to infectious microenvironments for sepsis management. *Adv Mater*. 2018;30 (43):1803618. doi:10.1002/adma.201803618
50. Lv X, Zhang J, Yang D, et al. Recent advances in pH-responsive nanomaterials for anti-infective therapy. *J Mat Chem B*. 2020;8 (47):10700–10711. doi:10.1039/D0TB02177F
51. Song S, Wang Y, Xie J, et al. Carboxymethyl chitosan modified carbon nanoparticle for controlled emamectin benzoate delivery: improved solubility, ph-responsive release, and sustainable pest control. *ACS Appl Mater Interfaces*. 2019;11(37):34258–34267. doi:10.1021/acsami.9b12564
52. Li T, Lü S, Yan J, Bai X, Gao C, Liu M. An environment-friendly fertilizer prepared by layer-by-layer self-assembly for pH-responsive nutrient release. *ACS Appl Mater Interfaces*. 2019;11(11):10941–10950. doi:10.1021/acsami.9b01425
53. Zhou X, Wang J, Fang W, et al. Genipin cross-linked type II collagen/chondroitin sulfate composite hydrogel-like cell delivery system induces differentiation of adipose-derived stem cells and regenerates degenerated nucleus pulposus. *Acta Biomater*. 2018;71:496–509. doi:10.1016/j.actbio.2018.03.019
54. Xu X, Gu Z, Chen X, et al. An injectable and thermosensitive hydrogel: promoting periodontal regeneration by controlled-release of aspirin and erythropoietin. *Acta Biomater*. 2019;86:235–246. doi:10.1016/j.actbio.2019.01.001
55. Castro Dos Santos NC, Andere NMRB, Araujo CF, et al. Omega-3 PUFA and aspirin as adjuncts to periodontal debridement in patients with periodontitis and type 2 diabetes mellitus: randomized clinical trial. *J Periodontol*. 2020;91(10):1318–1327. doi:10.1002/JPER.19-0613
56. Yang M, Li L, Soh Y, Heo SM. Effects of omega-3 fatty acids and aspirin on *Porphyromonas gingivalis*-induced periodontitis in rats. *J Periodontol*. 2019;90(11):1307–1319. doi:10.1002/JPER.19-0063
57. Xie Y, Pan M, Gao Y, Zhang L, Ge W, Tang P. Dose-dependent roles of aspirin and other non-steroidal anti-inflammatory drugs in abnormal bone remodeling and skeletal regeneration. *Cell Biosci*. 2019;9:103. doi:10.1186/s13578-019-0369-9
58. Wang F, Huang P, Huang D, et al. Preparation and functionalization of acetylsalicylic acid loaded chitosan/gelatin membranes from ethanol-based suspensions via electrophoretic deposition. *J Mat Chem B*. 2018;6(15):2304–2314. doi:10.1039/C7TB03033A
59. Yang Y, Shi K, Yu K, et al. Degradable hydrogel adhesives with enhanced tissue adhesion, superior self-healing, cytocompatibility, and antibacterial property. *Adv Healthc Mater*. 2022;11(4):2101504. doi:10.1002/adhm.202101504
60. Mosa IF, Youssef M, Kamel M, Mosa OF, Helmy Y. Synergistic antioxidant capacity of CsNPs and CurNPs against cytotoxicity, genotoxicity and pro-inflammatory mediators induced by hydroxyapatite nanoparticles in male rats. *Toxicol Res*. 2019;8(6):939–952. doi:10.1039/c9tx00221a
61. Kalgutkar AS, Crews BC, Rowlinson SW, Garner C, Seibert K, Marnett LJ. Aspirin-like molecules that covalently inactivate cyclooxygenase-2. *Science*. 1998;280(5367):1268–1270. doi:10.1126/science.280.5367.1268
62. Yang X, Li Y, Liu X, Zhang R, Feng Q. In vitro uptake of hydroxyapatite nanoparticles and their effect on osteogenic differentiation of human mesenchymal stem cells. *Stem Cells Int*. 2018;2018:2036176. doi:10.1155/2018/2036176
63. Hajiali H, Ouyang L, Llopis-Hernandez V, Dobre O, Rose F. Review of emerging nanotechnology in bone regeneration: progress, challenges, and perspectives. *Nanoscale*. 2021;13(23):10266–10280. doi:10.1039/D1NR01371H
64. Xia R, Geng G, Yu X, et al. LINC01140 promotes the progression and tumor immune escape in lung cancer by sponging multiple microRNAs. *J Immunother Cancer*. 2021;9(8):e002746. doi:10.1136/jitc-2021-002746
65. Daghrery A, Ferreira JA, Xu J, et al. Tissue-specific melt electrowritten polymeric scaffolds for coordinated regeneration of soft and hard periodontal tissues. *Bioact Mater*. 2023;19:268–281. doi:10.1016/j.bioactmat.2022.04.013
66. Liu J, Zhao Z, Ruan J, et al. Stem cells in the periodontal ligament differentiated into osteogenic, fibrogenic and cementogenic lineages for the regeneration of the periodontal complex. *J Dent*. 2020;92:103259. doi:10.1016/j.jdent.2019.103259
67. Fawzy El-Sayed KM, Elahmady M, Adawi Z, et al. The periodontal stem/progenitor cell inflammatory-regenerative cross talk: a new perspective. *J Periodont Res*. 2019;54(2):81–94. doi:10.1111/jre.12616
68. Greabu M, Giampieri F, Imre MM, et al. Autophagy, one of the main steps in periodontitis pathogenesis and evolution. *Molecules*. 2020;25 (18):4338. doi:10.3390/molecules25184338
69. Liu Y, Lin J, Wu X, et al. Aspirin-mediated attenuation of intervertebral disc degeneration by ameliorating reactive oxygen species in vivo and in vitro. *Oxidative Med Cell Longev*. 2019;2019:7189854. doi:10.1155/2019/7189854
70. Sun Y, Shu R, Li C-L, Zhang M-Z. Gram-negative periodontal bacteria induce the activation of toll-like receptors 2 and 4, and cytokine production in human periodontal ligament cells. *J Periodontol*. 2010;81(10):1488–1496. doi:10.1902/jop.2010.100004
71. Huang X, Chen H, Xie Y, Cao Z, Lin X, Wang Y. FoxO1 overexpression ameliorates TNF-α-induced oxidative damage and promotes osteogenesis of human periodontal ligament stem cells via antioxidant defense activation. *Stem Cells Int*. 2019;2019:2120453. doi:10.1155/2019/2120453
72. Amarasekara DS, Yun H, Kim S, Lee N, Kim H, Rho J. Regulation of osteoclast differentiation by cytokine networks. *Immune Netw*. 2018;18 (1):e8. doi:10.4110/in.2018.18.e8
73. Wongwichai T, Teeyakasem P, Pruksakorn D, Kongtawelert P, Pothacharoen P. Anthocyanins and metabolites from purple rice inhibit IL-1β-induced matrix metalloproteinases expression in human articular chondrocytes through the NF-κB and ERK/MAPK pathway. *Biomed Pharmacother*. 2019;112:108610. doi:10.1016/j.biopha.2019.108610
74. Curtis MA, Diaz PI, Van Dyke TE. The role of the microbiota in periodontal disease. *Periodontol*. 2020;83(1):14–25. doi:10.1111/prd.12296
75. Fiorillo L, Cervino G, Laino L, et al. *Porphyromonas gingivalis*, periodontal and systemic implications: a systematic review. *Dent J*. 2019;7 (4):114. doi:10.3390/dj7040114
76. Pye AD, Lockhart DEA, Dawson MP, Murray CA, Smith AJ. A review of dental implants and infection. *J Hosp Infect*. 2009;72(2):104–110. doi:10.1016/j.jhin.2009.02.010

77. Makvandi P, Josic U, Delfi M, et al. Drug delivery (nano)platforms for oral and dental applications: tissue regeneration, infection control, and cancer management. *Adv Sci*. 2021;8(8):2004014. doi:10.1002/advs.202004014
78. Li H, Yin D, Li W, Tang Q, Zou L, Peng Q. Polydopamine-based nanomaterials and their potentials in advanced drug delivery and therapy. *Colloids Surf B Biointerfaces*. 2021;199:111502. doi:10.1016/j.colsurfb.2020.111502
79. Yu D, Feng J, You H, et al. The microstructure, antibacterial and antitumor activities of chitosan oligosaccharides and derivatives. *Mar Drugs*. 2022;20(1):69. doi:10.3390/md20010069
80. Ke CL, Deng FS, Chuang CY, Lin CH. Antimicrobial actions and applications of chitosan. *Polymers*. 2021;13(6):904. doi:10.3390/polym13060904
81. Luz C, Calpe J, Saladino F, et al. Antimicrobial packaging based on ε-polylysine bioactive film for the control of mycotoxigenic fungi in vitro and in bread. *J Food Process Preserv*. 2018;42(1):e13370. doi:10.1111/jfpp.13370
82. Tan Z, Shi Y, Xing B, Hou Y, Cui J, Jia S. The antimicrobial effects and mechanism of ε-poly-lysine against *Staphylococcus aureus*. *Bioresour Bioprocess*. 2019;6(1):11. doi:10.1186/s40643-019-0246-8
83. Liu X, Camilleri ET, Li L, et al. Injectable catalyst-free "click" organic-inorganic nanohybrid (click-ON) cement for minimally invasive in vivo bone repair. *Biomaterials*. 2021;276:121014. doi:10.1016/j.biomaterials.2021.121014
84. Lee N-H, Kang MS, Kim T-H, et al. Dual actions of osteoclastic-inhibition and osteogenic-stimulation through strontium-releasing bioactive nanoscale cement imply biomaterial-enabled osteoporosis therapy. *Biomaterials*. 2021;276:121025. doi:10.1016/j.biomaterials.2021.121025
85. Filippi M, Dasen B, Guerrero J, et al. Magnetic nanocomposite hydrogels and static magnetic field stimulate the osteoblastic and vasculogenic profile of adipose-derived cells. *Biomaterials*. 2019;223:119468. doi:10.1016/j.biomaterials.2019.119468
86. Komori T. Regulation of proliferation, differentiation and functions of osteoblasts by Runx2. *Int J Mol Sci*. 2019;20(7):1694. doi:10.3390/ijms20071694
87. Yang SL, Guo ZY, Miao FP, Xue QZ, Qin S. The hydroxyl radical scavenging activity of chitosan, hyaluronan, starch and their O-carboxymethylated derivatives. *Carbohydr Polym*. 2010;82(4):1043–1045. doi:10.1016/j.carbpol.2010.06.014
88. Hu JF, Yang L, Yang P, Jiang SH, Liu XH, Li YW. Polydopamine free radical scavengers. *Biomaterials Science*. 2020;8(18):4940–4950. doi:10.1039/D0BM01070G
89. Chen Y, Luo RH, Li J, et al. Intrinsic radical species scavenging activities of tea polyphenols nanoparticles block pyroptosis in endotoxin-induced sepsis. *Acs Nano*. 2022;16(2):2429–2441. doi:10.1021/acsnano.1c08913
90. Ma Q, Jiang N, Liang S, et al. Functionalization of a clustered TiO2 nanotubular surface with platelet derived growth factor-BB covalent modification enhances osteogenic differentiation of bone marrow mesenchymal stem cells. *Biomaterials*. 2020;230:119650. doi:10.1016/j.biomaterials.2019.119650
91. Yi G, Zhang S, Ma Y, et al. Matrix vesicles from dental follicle cells improve alveolar bone regeneration via activation of the PLC/PKC/MAPK pathway. *Stem Cell Res Ther*. 2022;13(1):41. doi:10.1186/s13287-022-02721-6
92. Fattahi R, Mohebichamkhorami F, Khani MM, Soleimani M, Hosseinzadeh S. Aspirin effect on bone remodeling and skeletal regeneration: review article. *Tissue Cell*. 2022;76:101753. doi:10.1016/j.tice.2022.101753
93. Jiang Y, Qin H, Wan H, et al. Asprin-loaded strontium-containing α-calcium sulphate hemihydrate/nano-hydroxyapatite composite promotes regeneration of critical bone defects. *J Cell Mol Med*. 2020;24(23):13690–13702. doi:10.1111/jcmm.15918
94. Marquez-Grant N, Baldini E, Jeynes V, et al. How do drugs affect the skeleton? Implications for forensic anthropology. *Biology*. 2022;11(4):524. doi:10.3390/biology11040524
95. Van Dyke TE, Sima C. Understanding resolution of inflammation in periodontal diseases: is chronic inflammatory periodontitis a failure to resolve? *Periodontol*. 2020;82(1):205–213. doi:10.1111/prd.12317
96. Zupancic S, Kocbek P, Baumgartner S, Kristl J. Contribution of nanotechnology to improved treatment of periodontal disease. *Curr Pharm Des*. 2015;21(22):3257–3271. doi:10.2174/1381612821666150531171829
97. Li B, Sun J, Dong Z, et al. GCN5 modulates osteogenic differentiation of periodontal ligament stem cells through DKK1 acetylation in inflammatory microenvironment. *Sci Rep*. 2016;6:26542. doi:10.1038/srep26542
98. Chang J, Liu F, Lee M, et al. NF-kappa B inhibits osteogenic differentiation of mesenchymal stem cells by promoting beta-catenin degradation. *Proc Natl Acad Sci U S A*. 2013;110(23):9469–9474. doi:10.1073/pnas.1300532110
99. Lingappan K. NF-kappaB in oxidative stress. *Current Opinion in Toxicology*. 2018;7:81–86. doi:10.1016/j.cotox.2017.11.002
100. Li NX, Karin M. Is NF-kappa B the sensor of oxidative stress? *FASEB J*. 1999;13(10):1137–1143. doi:10.1096/fasebj.13.10.1137
101. Jimi E, Hirata S, Shin M, Yamazaki M, Fukushima H. Molecular mechanisms of BMP-induced bone formation: cross-talk between BMP and NF-κB signaling pathways in osteoblastogenesis. *Jpn Dent Sci Rev*. 2010;46(1):33–42. doi:10.1016/j.jdsr.2009.10.003
102. Kong X, Liu Y, Ye R, et al. GSK3β is a checkpoint for TNF-α-mediated impaired osteogenic differentiation of mesenchymal stem cells in inflammatory microenvironments. *Biochimica et Biophysica Acta*. 2013;1830(11):5119–5129. doi:10.1016/j.bbagen.2013.07.027
103. Cao Y, Xiong J, Mei S, et al. Aspirin promotes bone marrow mesenchymal stem cell-based calvarial bone regeneration in mini swine. *Stem Cell Res Ther*. 2015;6:210. doi:10.1186/s13287-015-0200-4
104. Padial-Molina M, Marchesan JT, Taut AD, Jin Q, Giannobile WV, Rios HF. Methods to validate tooth-supporting regenerative therapies. *Methods Mol Biol*. 2012;887:135–148. doi:10.1007/978-1-61779-860-3_13
105. Pellegrini G, Seol YJ, Gruber R, Giannobile WV. Pre-clinical models for oral and periodontal reconstructive therapies. *J Dent Res*. 2009;88(12):1065–1076. doi:10.1177/0022034509349748
106. Wang Y, Xiao QY, Zhong WJ, et al. Low-intensity pulsed ultrasound promotes periodontal regeneration in a beagle model of furcation involvement. *Front Bioengineering Biotechnol*. 2022;10:548.
107. Zhang X, Han N, Li G, et al. Local icariin application enhanced periodontal tissue regeneration and relieved local inflammation in a minipig model of periodontitis. *Int J Oral Sci*. 2018;10(2):19. doi:10.1038/s41368-018-0020-3